課程博士

2019 年 3 月

関西大学審査学位論文

Preparation and characterization of nonaqueous electrolyte from natural polymers for electric double-layer capacitors

天然高分子を用いた電気二重層キャパシタ用電解質の調製及びキャラクタリゼーション

研究科・専攻：理工学研究科・総合理工学専攻

研究領域　：　生体材料化学

学籍番号　：　16D6010

氏名　　：　コタタ　ディトポン

博士論文要旨

理工学研究科総合理工学専攻
研究領域：生体材料化学
学籍番号： 16D6010
氏名：コタタ　ディトポン

【論題】：Preparation and characterization of nonaqueous electrolyte from natural polymers for electric double-layer capacitors
(天然高分子を用いた電気二重層キャパシタ用電解質の調製及び
キャラクタリゼーション)

【概要】

Electric double-layer capacitors (EDLCs) are electrochemical devices that have received much attention in recent years because of their outstanding properties of long cycle lifetime and high sustained power density. Ionic liquid (IL) is considered to be promising electrolyte for EDLCs. Many researchers have been trying to prepare IL as solution electrolytes in the EDLCs due to their excellent properties, for example, near-zero vapor pressure, high thermal stability and non-flammability. However, the liquid leakage and safety issue are considered for IL electrolytes in the EDLCs system. Hence, non-aqueous electrolyte is more interesting for EDLCs. The various gel-electrolyte including IL have been prepare.

Regarding the requirement of sustainable development and non-renewable resources depletion, application of natural polymers has attracted significant attention. The development of biomass for polymer electrolytes has been widely studied in these recent year such as chitosan, alginate, bacterial cellulose, gelatin, carrageen, agar, starch, natural rubber, pectin, or polysaccharide of gar gum.

In this research, we focus on preparation and characterization of novel electrolytes from natural polymers including IL of 1-ethyl-3-methylimidazolium tetrafluoroborate ($EMImBF_4$) for use as non-aqueous electrolytes in EDLC. The new electrolytes in this research were successfully prepared from 3 systems; (i) bacterial cellulose coated with alternating layers of

chitosan/alginate, (ii) chitosan thin-film and (iii) gelatin nanofiber electrospinning. Moreover, there obtained samples were fabricated in EDLC test cell for electrochemical properties measurement by charge–discharge performance, discharge capacitance and alternative impedance for application test.

【各章の要旨】

In chapter 1, general introduction and background describing about EDLC and IL including the brief detail of natural polymers which was used for preparing nonaqueous electrolyte in this research; bacterial cellulose, chitosan, alginate and gelatin.

In chapter 2, A novel gel electrolyte has been prepared using bacterial cellulose (BC) coated with chitosan (CTS) and alginate (Alg) layers, which contain 1-ethyl-3-methylimidazolium tetrafluoroborate ($EMImBF_4$). The inoculated BC was oxidized and coated with alternating layers of CTS and Alg via ionic crosslinking to produce the gel electrolytes. The CTS content of the obtained gel electrolytes linearly increased with an increase in the number of CTS and Alg layers on the BC fibers. The results imply that the CTS and Alg layers successfully bound onto each fiber of BC, which was consistent with FTIR measurements. Based on a structural analysis, the fabricated gel electrolytes had a nanofibrous structure with a fiber diameter range of approximately 78.6–99.0 nm, a high thermal stability, and a significantly improved tensile strength compared to gel electrolytes of only CTS or Alg. In addition, the EDLCs test cell with a gel electrolyte of BC coated with 15 layers of CTS and Alg containing $EMImBF_4$ showed a high discharge capacitance, implying that the high affinity of this gel electrolyte for the activated-carbon electrode leads to reduced electrode/electrolyte interfacial resistance, which shows the potential of this approach compared with liquid-phase $EMImBF_4$ to obtain high-performance, safety-oriented EDLCs.

In chapter 3, A novel thin-film electrolyte (TFE) based on chitosan (CS) with $EMImBF_4$ was prepared by a new procedure. In this system, $EMImBF_4$ plays important roles as both a dissolving solution and a charge carrier for EDLC application. Through analysis and characterization of the obtained products, the CS-TEFs showed a surface without separation of phase between CS and $EMImBF_4$. The FT-IR spectra revealed peaks which are characteristic of CS including $EMImBF_4$ that confirm an effective introduction of $EMImBF_4$ into the CS matrix. The thermograms and tensile testing results indicated that these CS-TEFs had high thermal

stabilities with good tensile strength, which is a favorable property for solid-electrolyte to be used in EDLCs. Moreover, the EDLCs test cell with CS-TFE with a calculated dry thin-film content of 80 wt% $EMImBF_4$ showed a comparable IR drop and higher discharge capacitance than a liquid-phase $EMImBF_4$ system and also showed low electrode/electrolyte interfacial resistance. Consequently, this novel CS-TFE is suitable for high-performance EDLCs and improves the safety of such devices.

In chapter 4, A novel nanofibrous gel electrolyte was prepared via gelatin electrospinning to be used as a nonaqueous electrolyte in EDLCs. An electrospinning technique with a 25 wt% gelatin solution was used to produce gelatin electrospun (GES) electrolytes. A structural analysis of the GES products showed a clearly nanofibrous structure having fiber diameters in the range of approximately 306.2–428.4 nm, high thermal stability, high tensile strength, and resistance to damage upon immersion in $EMImBF_4$. After testing a range of spinning times, GES electrolytes that were electrospun with 25 min of spinning time (GES-25) were used to fabricate EDLC test cells with $EMImBF_4$. These test cells were compared with test cells using gelatin films containing $EMImBF_4$ and with testing cells using pure $EMImBF_4$ with a separator as the electrolyte. The test cell with the GES-25/$EMImBF_4$ gel electrolyte showed a similar IR drop and discharge capacitance as the liquid-$EMImBF_4$ test cell. However, the electronic contact resistance in activated carbon electrode at the electrode/electrolyte interface was significantly better in the GES-25/$EMImBF_4$ test cell compared with the test cell with the gelatin film/$EMImBF_4$ electrolytes. The results demonstrate that this novel nonaqueous gel electrolyte can be used for solid-stage electrolyte in EDLCs to improve the safety of such devices.

Table of Contents

Preparation and characterization of nonaqueous electrolyte from natural polymers for electric double-layer capacitors

Page

Chapter 1
General Introduction

1.1. Scope of this research

Electronic technologies combined with the demand of high energy and power storage devices are manufactured in compact and handy-to-use way without dropping their performance. Electrochemical double layer capacitors (EDLCs) can be functional and meet the requirements. It's a good alternative to any applications that requires energy storage because of the advantages; charging efficiency, fast response, long life time, and wide operating temperature range [1–5].

Ionic liquid (IL) is considered to be promising electrolyte for EDLCs. Many researchers have been trying to prepare IL as solution electrolytes in the EDLCs [6–11] due to their excellent properties, for example, near-zero vapor pressure, high thermal stability and non-flammability [12–14]. However, the liquid leakage and safety issue are considered for IL electrolytes in the EDLCs system. Hence, non-aqueous electrolyte is more interesting for EDLCs. The various gel-electrolyte including IL have been prepare [15–22].

Regarding the requirement of sustainable development and non-renewable resources depletion, application of natural polymers has attracted significant attention. The development of biomass for polymer electrolytes has been widely studied in these recent year such as chitosan [23–25], alginate [25–28], cellulose [29], carrageen [30–33], agar [34, 35], starch [36–38], natural rubber [39–40], pectin [41], and polysaccharide of gar gum [42].

In this research, we focus on preparation and characterization of novel electrolytes from natural polymers including IL of 1-ethyl-3-methylimidazolium tetrafluoroborate ($EMImBF_4$) for use as non-aqueous electrolytes in EDLC. The new electrolytes in this research were prepared from 3 systems; (i) bacterial cellulose coated with alternating layers of chitosan/alginate, (ii) chitosan thin-film and (iii) gelatin nanofiber electrospinning. Moreover, the obtained samples were fabricated in EDLC test cell for electrochemical properties measurement by the charge–discharge performance, discharge capacitance and alternative impedance for application test.

1.2. Electrochemical double layer capacitor (EDLC)

1.2.1. Brief overview of EDLC

Electrochemical double layer capacitors (EDLCs), alternatively know as super capacitors or ultracapacitors, represent a class of energy storage devices that are capable of storing electrical energy converted from sustainable sources. They are distinguished from other energy storage devices by a number of unique characteristics. For example, they can achieve much higher power densities than rechargeable batteries, and they have higher energy densities compared to conventional dielectric capacitors [1–5]. The Ragone plot [43] as shown in Fig. 1 shows the comparison of different storage technologies and Table 1 shows the properties comparison of EDLC, capacitor and batteries [44].

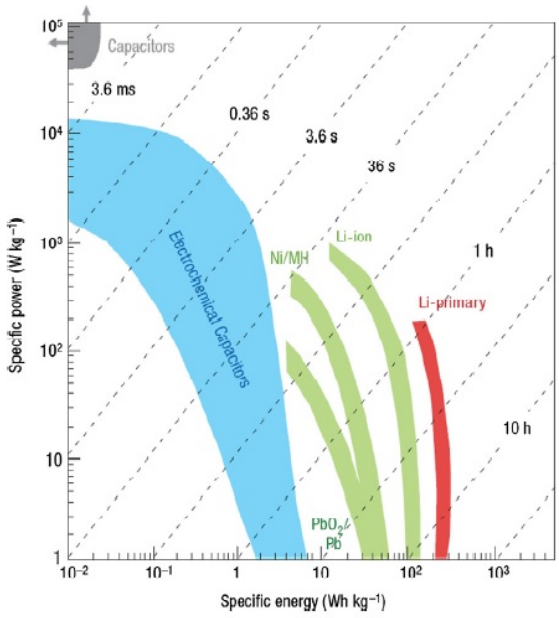

Fig. 1 Plots of gravimetric power density vs. gravimetric energy density (Ragone plot) of various energy storage devices. Values are normalized to the total weight of the device. Dotted lines represent the time needed to fully charge or discharge a device [43].

Table 1 Properties comparison of EDLC, capacitor and batteries [44].

Parameter	EDLC	Capacitors	Batteries
Energy Storage	W-Sec of energy	W-Sec of energy	W-Hr of energy
Charge Method	voltage across terminals	voltage across terminals	current and voltage
Power Delivered	rapid discharge, linear or exponential voltage decay	rapid discharge, linear or exponential voltage decay	constant voltage over long time period
Charge/Discharge Time	msec to sec	psec to msec	1 to 10 hrs
Form Factor	small	small to large	large
Weight	1–2 g	1 g to 10 kg	1 g to >10 kg
Energy Density	1 to 5 Wh/kg	0.01 to 0.05 Wh/kg	8 to 600 Wh/kg
Power Density	High, >4000W/kg	High, >5000W/kg	Low, 100–3000 W/kg
Operating Voltage	2.3–2.8 V/cell	6–800 V/cell	1.2–4.2 V/cell
Lifetime	>100k cycles	>100k cycles	150 to 1500 cycles
Operating Temp	-40 to 85 °C	-20 to 100 °C	-20 to 65 °C

Moreover, the basic schematics comparison of EDLC and lithium ion battery is shown in Fig. 2. Batteries store charge through the conversion of electrical energy onto chemical energy. Rechargeable secondary batteries use reactions that are reversible (e.g. lithium ion intercalation into graphite) [45–46]. In contrast to batteries, charge storage in supercapacitors is non-faradaic and occurs by the physical adsorption and desorption of ions inside the carbon electrode pores when an external voltage is applied. As electronic charge accumulates in an electrode, it is balanced at the interface by an equal and opposite ionic charge in the electrolyte [47] which is the mechanism of ion absorption and desorption to the electrical double layer contributes to the charge and discharge of EDLC is shown in Fig. 3. The physical mechanism of charge storage gives rise to fast charge and discharge times and long cycle lives, characteristic properties that make supercapacitors attractive devices to complement batteries.

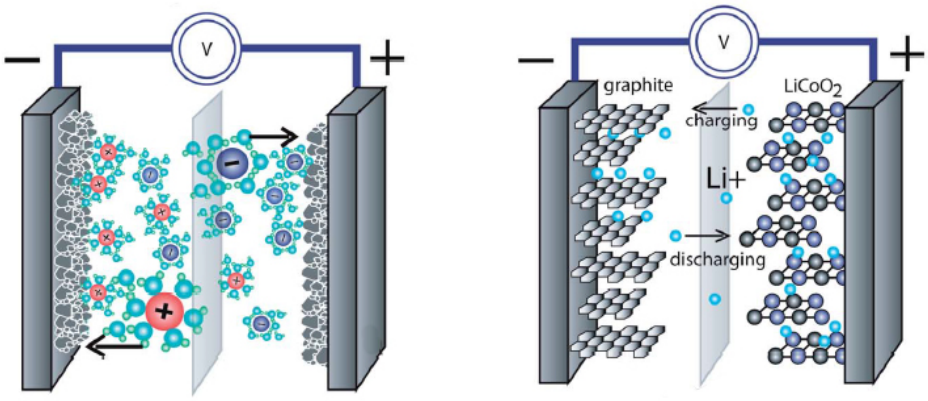

Fig. 2 Basic schematics of (a) EDLC and (b) lithium ion battery [46].

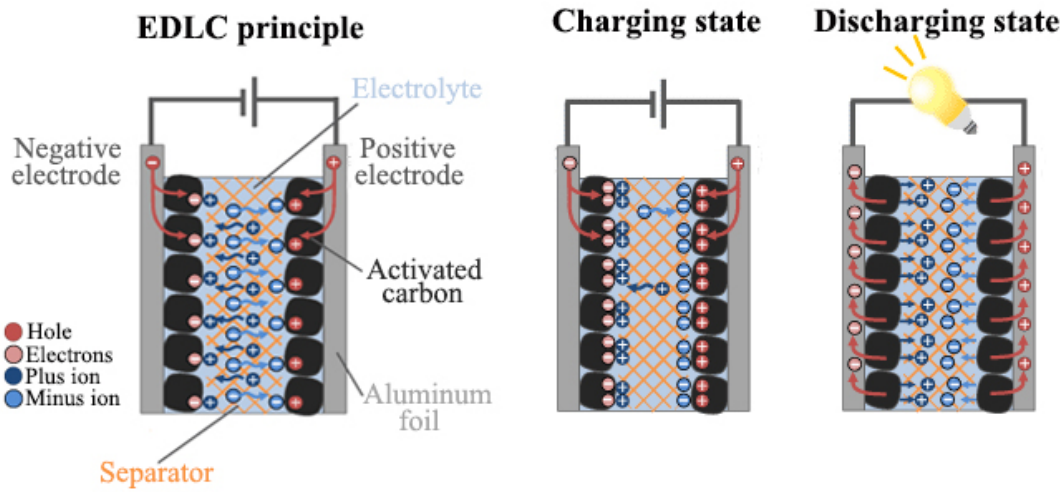

Fig. 3 EDLC principle and charge-discharge mechanism.

1.2.2. EDLC construction

A wide variety of EDLC materials and processes for cell construction currently exist. The Schematic view of a supercapacitor is shown in Fig. 4.

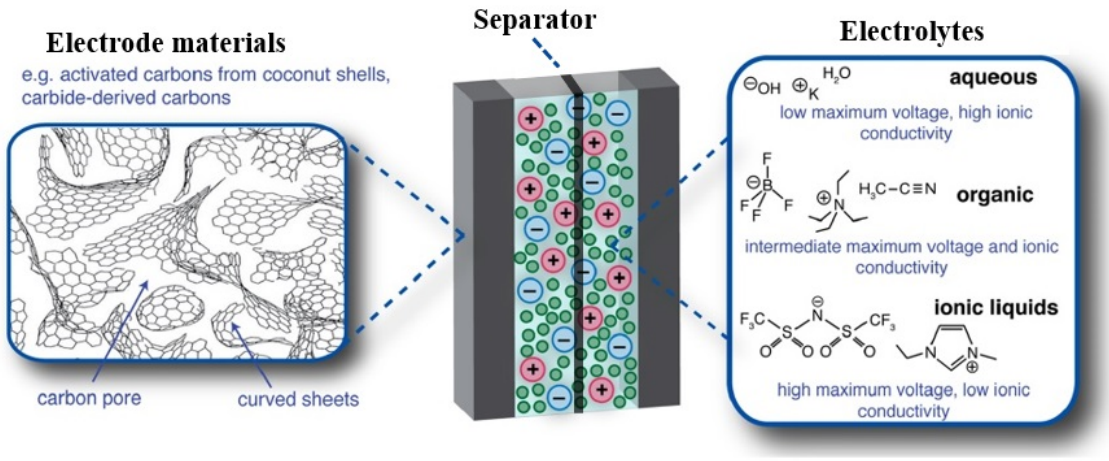

Fig. 4 Schematic view of EDLC including electrode materials, electrolytes and separator [47].

1.2.2.1. Electrode materials

Porous carbon electrode materials are generally used as electrode material. It was prepared by the heat treatment and subsequent chemical activation of organic materials, such as coconut shells and wood [47], whereas a related class of materials, carbide-derived carbons (CDCs), are obtained from metal carbides by extracting the metal atoms [48]. Moreover, more exotic materials e.g. carbon nanotubes and graphenes are also being developed for supercapacitor application. However, porous carbon electrodes can take a number of manufactured forms such as foams, fibers, and nanotubes and it is still an attractive option because of its low cost, availability, and long history of use [1].

1.2.2.2. Electrolytes

There are currently 3 types of electrolyte in widely use in EDLC; organic solvents, aqueous and ionic liquid (IL). The most commonly electrolytes used in the commercial devices are comprised of salts dissolved in organic solvents (e.g., tetraethylammonium tetrafluoroborate in acetonitrile solvent, $NEt_4{-}BF_4$/CAN) due to the organic solvents provide a good balance of relatively large maximum operating voltages about 2.5 V and high ionic conductivities about 20–60 mS/cm. Aqueous electrolytes have a lower breakdown voltage,

typically about 1 V, but have better conductivity than organic electrolytes. Moreover, IL are very interesting for alternatively electrolytes because of high operating voltages (about 4 V) [49–51].

The capacitance of an EDLC is greatly influenced by the choice of electrolyte. The ability to store charge is dependent on the accessibility of the ions to the porous surface-area, so ion size and pore size must be optimal. The best pore size distribution in the electrode depends upon the size of the ions in the electrolyte, so both electrode and electrolyte must be chosen together [1].

1.2.2.3. Separator

The separator prevents the occurrence of electrical contact between the two electrodes, but it is ion-permeable, allowing ionic charge transfer to take place. For best EDLC performance the separator should have a high electrical resistance, a high ionic conductance, and a low thickness [1]. Polymer or paper separators are widely used for organic electrolytes, while ceramic or glass fiber separators are often used with aqueous and IL electrolytes.

1.2.2.4. Application and type of EDLC

Regarding high energy and power density of EDLC, some new applications of EDLC are being developed at an increasing rate such as memory back-up, electric vehicles, portable power supplies, electrochemical actuators and adjustable-speed drives.

EDLC are divided into the following categories, according to their shape and construction. Examples of EDLC type are shown in Fig. 5 and summary of structures and shape, capacitance and main applications of EDLC are shown in Table 2.

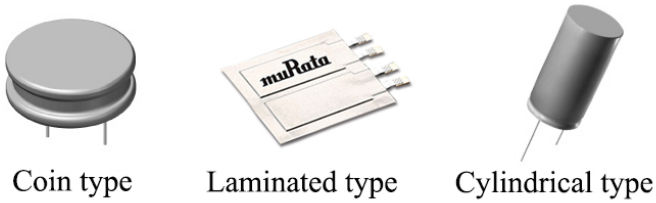

Fig. 5 type of EDLC [52]

Table 2 Summary of structures and shape, capacitance and main applications of EDLC [52].

Structures and shape	Capacitance	Main applications
Chip type	Ultra-low capacitance, 0.1 F and less	Clock and memory backup in various electronic devices
Coin type		Standby power for home appliances and A/V equipment
Laminated type	Low capacitance, 0.1 to 1 F	Battery load leveling in mobile devices, high-brightness LED flash assist current, momentary power loss protection, energy harvesting
Cylindrical type	Medium capacitance, 1 to 100 F	Road marking studs, LED signs, drive power for compact motors in toys
Modules (large number of interconnected cylindrical or rectangular cells)	High capacitance, 100 F and above	Energy regeneration in industrial equipment and automobiles, UPS equipment, emergency power supply for wind power generation control

1.3. Ionic liquid (IL)

Ionic Liquids (ILs) are room-temperature molten salts mostly composed of organic cations and (in)organic anions, which is in liquid state below 100 °C with nearly unlimited structural diversity and physicochemical variations through appropriate selection and modification of the cations and anions [53]. Information about IL can be found in the literature with a lot of key word such as room temperature molten salt, low-temperature molten salt, ambient-temperature molten salt, liquid organic salt or simple ionic liquid [3].

Due to the advantage of IL as nonflammability, nonvolatility and high thermal stability compare with conventional organic liquid electrolytes. IL have been extensively investigated as potential electrolytes for various electrochemical devices; rechargeable lithium cells [54, 55], solar cells [56–58], actuators [59] involved EDLC [6–11]. At first, many researchers focused on 1-ethyl-3-methylimidazolium tetrafluoroborate ($EMImBF_4$), structure is shown in Fig. 6, as

electrolytes for EDLC because it has a relatively low viscosity and high ionic conductivity [8, 9]. Then, there has been extensive synthesis of different families of IL composed of different anions and cations as shows in Fig. 7.

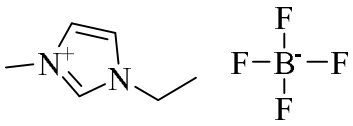

Fig. 6 Structure of 1-ethyl-3-methylimidazolium tetrafluoroborate ($EMImBF_4$)

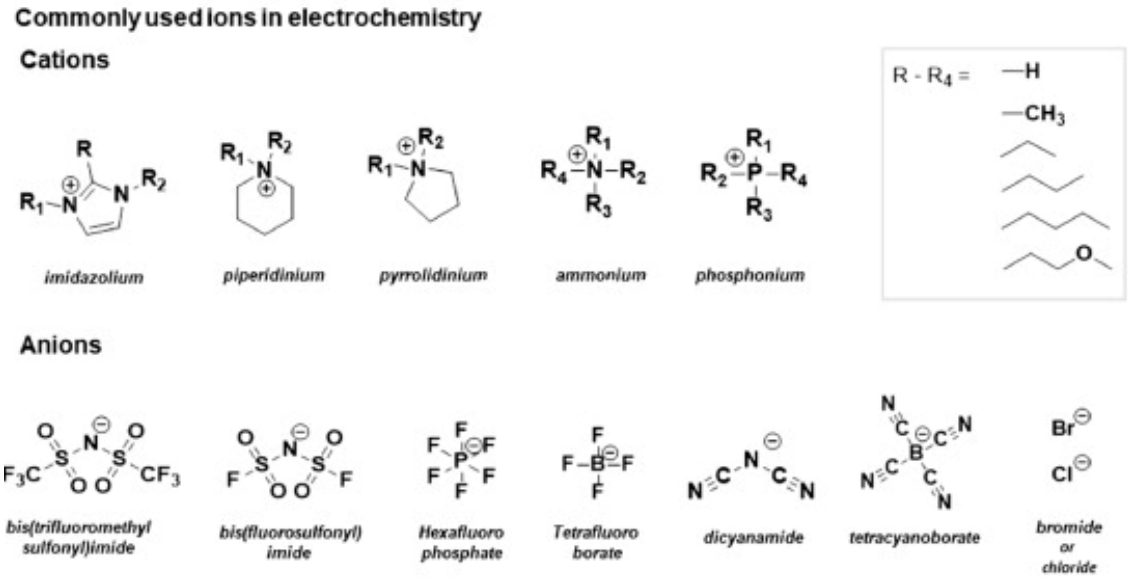

Fig. 7 Structures of some cations and anions of IL commonly used in electrochemistry [60]

1.4. Natural polymers

The natural polymers were used as raw material for preparation of nonaqueous electrolyte in this research; bacterial cellulose, chitosan, alginate and gelatin. A brief detail of them are being discussed in this section:

1.4.1. Bacterial cellulose

Bacterial cellulose (BC) is a natural pure cellulose aggregate, which consists of random assembled nanofibrils less than 100 nm [61–63], produced by strains of the gram-negative bacteria species such as *Acetobacter*, *Azotobacter*, *Rhizobium*, *Pseudomonas*, *Salmonella*, *Alcaligenes*, and gram-positive bacteria species such as *Sarcina ventriculi* [64]. The molecular formula of BC $(C_6H_{10}O_5)_n$, having a β-1,4 linkage between two glucose molecules (structure is shown in Fig. 8), is the same as that of plant cellulose but their physical and chemical features are different. Compared to plant cellulose, BC is more promising in the applications of engineered polymer nanocomposites, functional membranes, tissue engineering and electronic devices due to its unique structural advantages such as high degree of polymerization, high crystallinity and well-defined high surface area nanofibrillar network [65]. In addition, BC also displays unique physico-chemical properties including good biocompatibility, high water absorption capacities and high tensile strength [66].

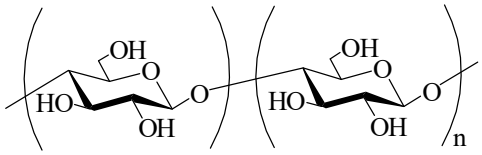

Fig. 8 Structures of cellulose

1.4.2. Chitosan

Chitosan, a cationic biopolymer, is the derivative of chitin. It is natural abundant resource second to cellulose [67, 68] present in outer shell of crustacean, exoskeleton of insect, and cell walls of some fungi [69–74]. Chitosan is a linear co-polymer composed of β(1→4) glucosamine and N-acetyl glucosamine residues (structure is shown in Fig. 9) [75]. It is produced in the process of either the chemical or enzymatic deacetylation of chitin [76]. The number of aliphatic amino groups is described by the degree of deacetylation (DDA). The higher the number is, the more free amino residues are present in the polymer chain [77]. Due to its reactive

amino groups, chitosan has many commercial applications; biomedical, pharmaceutical and electrical applications [23–25, 78].

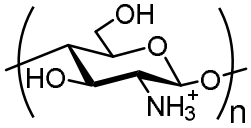

Fig. 9 Structures of chitosan

1.4.3. Alginate

Alginate is an anionic polysaccharide produced from marine brown algae and is partly responsible for the flexibility of seaweed. Commercial alginates are extracted from three species of brown algae are *Laminaria hyperborean*, *Ascophyllum nodosum*, and *Macrocystis pyrifera*; in which alginate comprises up to 40% of the dry weight. It is a linear polymer composed of (1 → 4)-linked D-mannuronic acid (M) and L-guluronic acid (G) units arranged either in homo- or hetero-polymeric form (structure is shown in Fig. 10 and 11) [79, 80]. The alginate properties depend on the proportion and sequence of M and G, and polymer chain length [80, 81]. Alginate exists as a mixed salt of various cations found in the seawater such as Mg^{2+}, Sr^{2+}, Ba^{2+}, and Na^{+}. The most important property of alginates is their ability to form gels by reaction with divalent cations such as Ca^{2+}. Alginate beads can be prepared by extruding a solution of sodium alginate containing the desired protein, as droplets, in to a divalent cross-linking solution such as Ca^{2+}, Sr^{2+}, or Ba^{2+} [81].

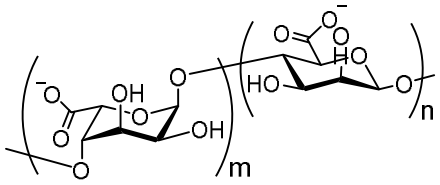

Fig. 10 Structures of alginate

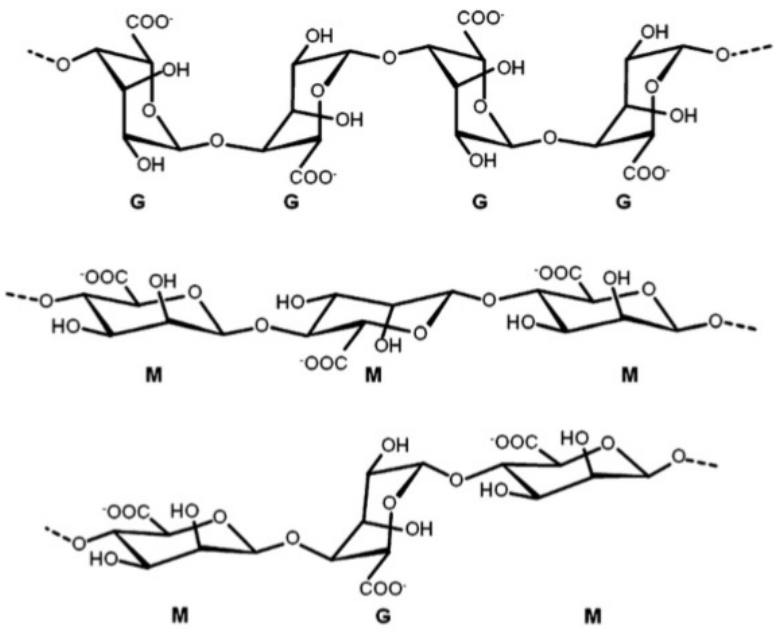

Fig. 11 Structures of G, M unit and alternating block in alginate [80].

1.4.4. Gelatin

Gelatin is a natural polymer and a fibrous protein that is present in the skin and bones of animals. It is a protein derived from the chemical degradation of collagen, with average molecular weights from 65,000 to 300,000 g/mol, depending on the grade of hydrolysis. Gelatin contains mainly glycine, proline and 4-hydroxyproline (for pigskin gelatin 33%, 13% and 9%, respectively) which structure is shown in Fig. 12 [82]. Gelatin is a biocompatible protein, and when it enters living body, shows low anti-genecity and very high bio-absorptivity. It is an important product, which has many applications in the food industry, particularly as a gelling agent, stabiliser and thickener, as well as in the medical and cosmetic industries [83].

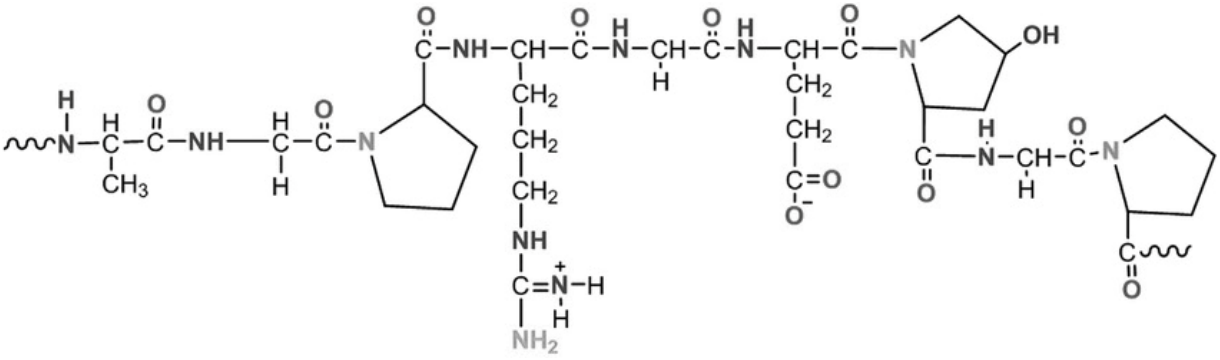

Fig. 12 Structures of gelatin [82]

1.5. Content of this thesis

This thesis is composed of five chapters shown below;

Chapter 1 is a general introduction and background.

Chapter 2 presents preparation and characterization of gel electrolyte with bacterial cellulose coated with alternating layer of chitosan and alginate. The inoculated bacterial cellulose was oxidized and coated with alternating layers of chitosan and alginate via ionic crosslinking to produce the gel electrolytes.

Chapter 3 presents preparation and characterization of thin-film electrolyte from chitosan. A novel thin-film electrolyte was prepared for chitosan with ionic liquid of $EMImBF_4$ by a new procedure. In this system, $EMImBF_4$ plays important roles as both a dissolving solution and a charge carrier for EDLC application.

Chapter 4 describes about preparation and characterization of electrospun gelatin nanofiber electrolyte. A novel nanofibrous gel electrolyte was prepared via gelatin electrospinning. An electrospinning technique with a 25 wt% gelatin solution was used to produce gelatin electrospun electrolytes by difference spinning time.

Chapter 5 is the conclusion of this thesis. The approach to fabricate nonaqueous electrolytes for use in EDLC are summarized.

1.6. References

[1] P. Sharma, T.S. Bhatti, Energy Convers. Manage. 51, 2901–2912 (2010)

[2] M. Winter, R. J. Brodd, Chem. Rev. 104, 4245–4269 (2004)

[3] M. Galiński, A. Lewandowski, I. Stępniak, Electrochim. Acta 51, 5567–5580 (2006)
[4] M. Tokita, N. Yoshimoto, K. Fujii, M. Morita, Electrochim. Acta 209, 210–218 (2016)
[5] Y. Song, T. Liu, F. Qian, C. Zhu, B. Yao, E. Duoss, C. Spadaccini, M. Worsley, Y. Li, J. Colloid Interface Sci. 509, 529–545 (2018)
[6] A. Lewandowski, M. Galiński, J. Phys. Chem. Solids 65, 281–286 (2004)
[7] Z. Zhou, M. Takeda, M. Ue, J. Fluorine Chem. 125, 471–476 (2004)
[8] T. Sato, G. Masuda, K. Takagi, Electrochim. Acta 49, 3603–3611 (2004)
[9] K. Yuyama, G. Masuda, H. Yoshida, T. Sato, J. Power Sources 162, 1401–1408 (2006)
[10] C.O. Ania, J. Pernak, F. Stefaniak, E. Raymundo-Piñero, F. Béguin, Carbon 44, 3126–3130 (2006)
[11] N. Handa, T. Sugimoto, M. Yamagata, M. Kikuta, M. Kono, M. Ishikawa, J. Power Sources 185, 1585–1588 (2008)
[12] X. Mu, X. Yang, D. Zhang, C. Liu, Carbohydr. Polym. 146, 46–51 (2016)
[13] W. Wang, J. Zhu, X. Wang, Y. Huang, Y. Wang, J. Macromol. Sci., Part B 49 (3), 528–541 (2010)
[14] K. Wilpiszewska, T. Spychaj, Carbohydr. Polym. 86, 424–428 (2011)
[15] M.M. Rao, J.S. Liu, W.S. Li, Y. Liang, D.Y. Zhou, J. Membr. Sci. 322, 314–319 (2008)
[16] B. Rupp, M. Schmuck, A. Balducci, M. Winter, W. Kern, Eur. Polym. J. 44, 2986–2990 (2008)
[17] M. Rao, X. Geng, Y. Liao, S. Hu, W. Li, J. Membr. Sci. 399-400, 37–42 (2012)
[18] R. Prasanth, N. Shubha, H.H. Hng, M. Srinivasan, Eur. Polym. J. 49, 307–318 (2013)
[19] K. Karuppasamy, P.A. Reddy, G. Srinivas, A. Tewari, R. Sharma, X.S. Shajan, D. Gupta, J. Membr. Sci. 514, 350–357 (2016)
[20] P.F.R. Ortega, J.P.C. Trigueiro, G.G. Silva, R.L. Lavall, Electrochim. Acta 188, 809–817 (2016)
[21] M. Safa, A. Chamaani, N. Chawla, B. El-Zahab, Electrochim. Acta 213, 587–593 (2016)
[22] J. Rymarczyk, M. Carewska, G.B. Appetecchi, D. Zane, F. Alessandrini, S. Passerini, Eur. Polym. J. 44, 2153–2161 (2008)
[23] K. Soeda, M. Yamagata, S. Yamazaki, M. Ishikawa, Electrochemistry 81(10), 867–872 (2013)

[24] M. Yamagata, K. Soeda, S. Ikebe, S. Yamazaki, M. Ishikawa, Electrochim. Acta 100, 275–280 (2013)

[25] M.Yamagata, K. Soeda, S. Ikebe, S. Yamazaki, M. Ishikawa, J. Electrochem. Soc. 41(22), 25–34 (2012)

[26] M. Yamagata, K. Soeda, S. Yamazaki, M. Ishikawa, J. Electrochem. Soc. 25(35), 193–200 (2010)

[27] M. Yamagata, S. Ikebe, Y. Kasai, K. Soeda, M. Ishikawa, J. Electrochem. Soc. 50(43), 27–36 (2013)

[28] K. Soeda, M. Yamagata, M. Ishikawa, J. Power Sources 280, 565–572 (2015)

[29] R. Ou, Y. Xie, X. Shen, F. Yuan, H. Wang, Q. Wang, J. Mater. Sci. 47, 5978–5986 (2012)

[30] N.N. Mobarak, N. Ramli, A. Ahmad, M.Y.A. Rahman, Solid State Ionics 224, 51–57 (2012)

[31] N.N. Mobarak, F.N. Jumaah, M.A. Ghani, M.P. Abdullah, A. Ahmad, Electrochim. Acta 175, 224–231 (2015)

[32] S. Rudhziah, M.S.A. Rani, A. Ahmad, N.S. Mohamed, H. Kaddami, Ind. Crops Prod. 72, 133–141 (2015)

[33] T.M.D. Palma, F. Migliardini, D. Caputo, P. Corbo, Carbohydr. Polym. 157, 122–127 (2017)

[34] E. Rapharl, C.O. Avellaneda, B. Manzolli, A. Pawlicka, Electrochim. Acta 55, 1455–1459 (2010)

[35] R. Leones, F. Sentanin, L.C. Rodrigues, I.M. Marrucho, J.M.S.S. Esperança, A. Pawlicka, M.M. Silva, Express Polym. Lett. 6 (12), 1007–1016 (2012)

[36] A.S.A. Khiar, A.K. Arof, Ionics 16, 123–129 (2010)

[37] M. Kumar, T. Tiwari, N. Srivastava, Carbohydr. Polym. 88, 54–60 (2012)

[38] M.F. Shukur, R. Ithnin, M.F.Z. Kadir, Electrochim. Acta 136, 204–216 (2014)

[39] A.M.M. Ali, R.H.Y. Subban, H. Bahron, T. Winie, F. Latif, M.Z.A. Yahya, Ionics 14, 491–500 (2008)

[40] S.N. Mohamed, N.A. Johari, A.M.M. Ali, M.K. Harun, M.Z.A. Yahya, J. Power Sources 183, 351–354 (2008)

[41] R.K. Mishra, A. Anis, S. Mondal, M. Dutt, A.K. Banthia, Chin. J. Polym. Sci. 27 (5), 639–646 (2009)

[42] Y.N. Sudhakar, M. Selvakumar, D. K. Bhat, Mater. Sci. Eng., B 180, 12–19 (2014)

[43] X. Zhang, H. Zhang, C. Li, K. Wang, X. Sun, Y. Ma, RSC Adv. 4, 45862–45884 (2014)

[44] T. Armstrong, *Emergency eCall – Available When You Need It*, [online] Available at: https://www.powersystemsdesign.com/articles/emergency-ecall-available-when-you-need-it/132/11691, [Accessed 12 Oct. 2018]

[45] V. Etacheri, R. Marom, R. Elazari, G. Salitra, D. Aurbach, Energy Environ. Sci. 4, 3243–3262 (2011)

[46] K. Jost, G. Dion, Y. Gogotsi, J. Mater. Chem. A 2, 10776–10787 (2014)

[47] A.C. Forse, C. Merlet, J.M. Griffin, C.P. Grey, J. Am. Chem. Soc. 138, 5731–5744 (2016)

[48] V. Presser, M. Heon, Y. Gogotsi, Adv. Funct. Mater. 21, 810–833 (2011)

[49] F. Béguin, V. Presser, A. Balducci, E. Frackowiak, Adv. Mater. 26, 2219–2251 (2014)

[50] A. Brandt, S. Pohlmann, A. Varzi, A. Balducci, S. Passerini, MRS Bull. 38, 554–559 (2013)

[51] A. Lewandowski, A. Olejniczak, M. Galinski, I. Stepniak, J. Power Sources 195, 5814–5819 (2010)

[52] TDK Techno Magazine Tech Mag., *TDK Techno Magazine*. [online] Available at: https://www.global.tdk.com/techmag/electronics_primer/vol8.htm, [Accessed 12 Oct. 2018].

[53] H. Liu, H. Yu, J. Mater. Sci. Technol. (2018), In Press.

[54] N. Nakagawa, S. Izuchi, K. Kuwana, T. Nukuda, Y. Aihara, J. Electrochem. Soc. 150, A695–A700 (2003)

[55] H. Sakaebe, H. Matsumoto, Electrochem. Commun. 5, 594–598 (2003)

[56] P. Wang, S.M. Zakeeruddin, I. Exnar, M. Grätzel, Chem. Commun. 24, 2972–2973 (2002)

[57] P. Wang, S.M. Zakeeruddin, P. Comte, I. Exnar, M. Grätzel, J. Am. Chem. Soc. 125, 1166–1167 (2003)

[58] H. Matsumoto, T. Matsuda, T. Tsuda, R. Hagiwara, Y. Ito, Y. Miyazaki, Chem. Lett. 30 (1), 26–27 (2001)

[59] D. Zhou, G.M. Spinks, G.G. Wallace, C. Tiyapiboonchaiya, D.R. MacFarlane, M. Forsyth, J. Sun, Electrochim. Acta 48, 2355–2359 (2003)

[60] V.L. Martins, R.M. Torresi, Curr. Opin. Electrochem. 9, 26–32 (2018)

[61] N. Halib, M. C. I. Amin and I. Ahmad, Sains Malaysiana 41 (2), 205–211 (2012)

[62] Y. Kaburagi, M. Ohoyama, Y. Yamaguchi, E. Shindou, A. Yoshida, N. Iwashita, N. Yoshizawa, M. Kodama, Carbon 55, 371–374 (2013)

[63] E.L. Hult, S. Yamanaka, M. Ishihara and J. Sugiyama, Carbohydr. Polym. 53, 9–14 (2003)

[64] M. Shoda, Y. Sugano, Biotechnol. Bioprocess. Eng. 10, 1–8 (2005)

[65] D. Tian, F. Shen, J. Hu, S. Renneckar, J.N. Saddler, Carbohydr. Polym. 198, 191–196 (2018)

[66] M.H. Kwak, J.E. Kim, J. Go, E.K. Koh, S.H. Song, H.J. Son, H.S. Kim, Y.H. Yun, Y.J. Jung, D.Y. Hwang, Carbohydr. Polym. 122, 387–398 (2015)

[67] M. Rinaudo, Prog. Polym. Sci. 31, 603–632 (2006)

[68] A. Domard, Carbohydr. Polym. 84, 696–703 (2011)

[69] R. Jayakumar, H. Nagahama, T. Furuike, H. Tamura, Int. J. Biol. Macromol. 42, 335–339 (2008)

[70] A. Anitha, V.V.D. Rani, R. Krishna, V. Sreeja, N. Selvamurugan, S.V. Nair, H. Tamura, R. Jayakumar, Carbohydr. Polym. 78, 672–677 (2009)

[71] K. Madhumathi, K.T. Shalumon, V.V.D. Rani, H. Tamura, T. Furuike, N. Selvamurugan, S.V. Nair, R. Jayakumar, Int. J. Biol. Macromol. 45, 12–15 (2009)

[72] H. Nagahama, H. Maeda, T. Kashiki, R. Jayakumar, T. Furuike, H. Tamura, Carbohydr. Polym. 76, 255–260 (2009)

[73] Y. Saito, V. Luchnikov, A. Inaba, K. Tamura, Carbohydr. Polym. 109, 44–48 (2014).

[74] T. Furuike, D. Komoto, H. Hashimoto, H. Tamura, Int. J. Biol. Macromol. 104, 1620–1625 (2017)

[75] C. Choi, J. Nam, J. Nah, J. Ind. Eng. Chem. 33, 1–10 (2016)

[76] I. Tsigos, A. Martinou, D. Kafetzopoulos, V. Bouriotis, Trends Biotechnol. 18(7), 305–312 (2000)

[77] A. Tiraferri, P. Maroni, D. Caro Rodríguez, M. Borkovec, Langmuir 30, 4980–4988 (2014)

[78] R. Jayakumar, M. Prabaharan, P.T. Sudheesh Kumar, S.V. Nair, H. Tamura, Biotechnol. Adv. 29, 322–337 (2011)

[79] J.H. Kim, S. Park, H. Kim, H.J. Kim, Y. Yang, Y.H. Kim, S. Jung, E. Kan, S.H. Lee, Carbohydr. Polym. 157, 137–145 (2017)

[80] K.Y. Lee, D.J. Mooney, Prog. Polym. Sci. 37, 106–126 (2012)

[81] M. George, T.E. Abraham, J. Controlled Release 114, 1–14 (2006)

[82] C. Peña, K. Caba, A. Eceiza, R. Ruseckaite, I. Mondragon, Bioresour. Technol. 101, 6836–6842 (2010)

[83] P. Likitdecharoj, J. Ratanavaraporn, J. Drug Deliv. Sci. Technol. 47, 367–374 (2018)

Chapter 2

Preparation and Characterization of Gel Electrolyte with Bacterial Cellulose Coated with Alternating Layers of Chitosan and Alginate

2.1. Introduction

With advances in electronic technologies, there is a demand for high-energy power-storage devices to be manufactured in a compact and handy-to-use way without a reduction in their performance. Electric double-layer capacitors (EDLCs), also known as supercapacitors, can be functional and meet the abovementioned requirements. The energy storage mechanism of EDLCs arises from non-faradic phenomena between two non-faradic electrodes and an electrolyte at their interfaces [1–3]. This can provide a higher sustained power density and longer charge–discharge cycle (>100,000 cycles) as compared with rechargeable battery systems [4, 5].

Owing to their excellent properties such as near-zero vapor pressure, high thermal stability, and non-flammability, ionic liquids (ILs), which have been widely promoted as green solvents [6–8], are being studied as electrolytes for EDLCs [9–14]. However, the liquid leakage and lack of safety associated with IL electrolytes in the EDLCs system must be considered. Hence, non-aqueous electrolytes are more promising for EDLCs. The various gel electrolytes, including IL-based electrolytes, have been prepared [15–22].

Considering depletion of nonrenewable resources, sustainable development and application of biodegradable polymers have attracted significant attention. In recent years, biomass such as carrageen [23–26], agar [27, 28], starch [29–31], and guar gum polysaccharide [32] have been developed for gel-polymer electrolytes. In addition, previous studies have reported successful preparation of gel electrolytes from chitosan (CTS) [33–35] and alginate (Alg) [35–38], including high-performance ILs for use in EDLCs. However, the low tensile strength of these gel electrolytes may be attributed to the properties of the materials used.

Bacterial cellulose (BC), which is natural polymer nanofiber, displays unique physical and chemical properties such as good biocompatibility, high water absorption capacity, high crystallinity, highly fibrous networks, and a high tensile strength and modulus [39, 40]. Therefore, if BC is used as the scaffold for CTS and Alg as a gel electrolyte, it is possible to efficiently combine both the higher tensile strength and the electrochemical properties of these materials.

In this chapter, a novel gel electrolyte was successfully prepared using BC coated with alternating layers of CTS and Alg including 1-ethyl-3-methylimidazolium tetrafluoroborate

($EMImBF_4$) for the use in EDLCs. The characterization of the gel electrolyte and its electrochemical properties were discussed.

2.2. Materials and methods

2.2.1. Materials

Gluconacetobacter xylinus ATCC 53582 was purchased from Summit Pharmaceuticals International Corporation (Japan). Chitosan (FL-80, Mw 90,000, degree of deacetylation (DDA): 89.7%) and sodium Alg (viscosity: 80–120 mPa s for 10 g/L at 20 °C) were supplied from Koyo Chemical Co., Ltd (Japan) and KIMICA corporation (Japan), respectively. 1-ethyl-3-methylimidazolium tetrafluoroborate ($EMImBF_4$, 99.0%) was purchased from Toyo Gosei Co., Ltd (Japan). Activated carbon (YP-50F), acetylene black (HS-100), sodium carboxymethyl cellulose (WS-C), and styrene-butadiene rubber (TRD2001) were purchased from Kuraray Co., Ltd (Japan), Denka company Ltd (Japan), DKS Co., Ltd (Japan), and JSR corporation (Japan), respectively. Other reagents were purchased from Wako Pure Chemical Company (Japan) and used without further purification.

2.2.2. Preparation of gel electrolytes of bacterial cellulose coated with alternating layers of CTS and Alg

2.2.2.1. Preparation of BC gel

The starting culture of *Gluconacet*obacter xylinus was inoculated at 30 °C for 7 days with 1 mL of *Gluconacetobacter xylinus* in 200 mL of Hestrin–Schramm (HS) medium containing 2% D-glucose, 0.5% yeast extract, 0.5% peptone, 0.115% sodium hydrogen phosphate, and 0.27% citric acid in deionized (DI) water (w/v) [41, 42]. The HS medium was sterilized at 121 °C for 15 min before use [43]. After the incubation period, BC was cultured at room temperature for 3 days by adding 1 mL of starter culture in 20 mL of HS medium. Subsequently, the obtained BC gel was washed with DI water to remove the HS medium and was treated in a 0.5 M sodium hydroxide (NaOH) solution at 90 °C for 1 h to eliminate bacterial

cells [40]. Then, the treated BC gel was washed with DI water until the pH of the filtrate was neutral before using the gel in future processes.

2.2.2.2. Preparation of BC coated with alternating layers of CTS and Alg

The BC nanofiber was oxidized with potassium periodate (KIO_4) before coating it with CTS and Alg. The BC was submerged in 400 mL of a 1-mg/mL KIO_4 solution and was stirred at 60 °C for 1 h [44]. The oxidized BC was then washed with DI water several times to remove the KIO4; then, it was soaked in DI water overnight at room temperature before coating with CTS and Alg in the next step. The oxidized BC was coated with layer-by-layer of CTS and Alg as follows: The CTS and Alg solutions were prepared with a concentration of 0.1% (w/v). The CTS solution was prepared by adding 0.4 g of CTS powder to a 2% (v/v) aqueous acetic acid and completing the volume to 400 mL and by subsequent stirring at 60 °C for 1 h. Meanwhile, the Alg solution was prepared by adding 0.4 g of Alg powder to DI water and completing the volume to 400 mL and by subsequent stirring at 60 °C for 1 h. Subsequently, the oxidized BC was submerged in 400 mL of the 0.1% (w/v) CTS solution and was stirred at 60 °C for 1 h to coat it with a layer of CTS. Then, the CTS-coated oxidized BC was submerged in 400 mL of the0.1% (w/v) Alg solution and was stirred at 60 °C for 1 h to coat it with a layer of Alg. Accordingly, the sample was coated with additional CTS layers alternated with Alg layers.

The coated sample was washed in 400 mL of DI water in an ultrasonic machine twice before repeated CTS or Alg coatings. A schematic of the coating method is shown in Fig. 1, and the number of coating layers of the samples are shown in Table 1. After coating, the sample thickness was reduced via pressing with a 2-kg load for 2 h; then, it was soaked in 400 mL of methanol for 3 days; the methanol bath was changed every day. The sample thus obtained was used in the subsequent steps.

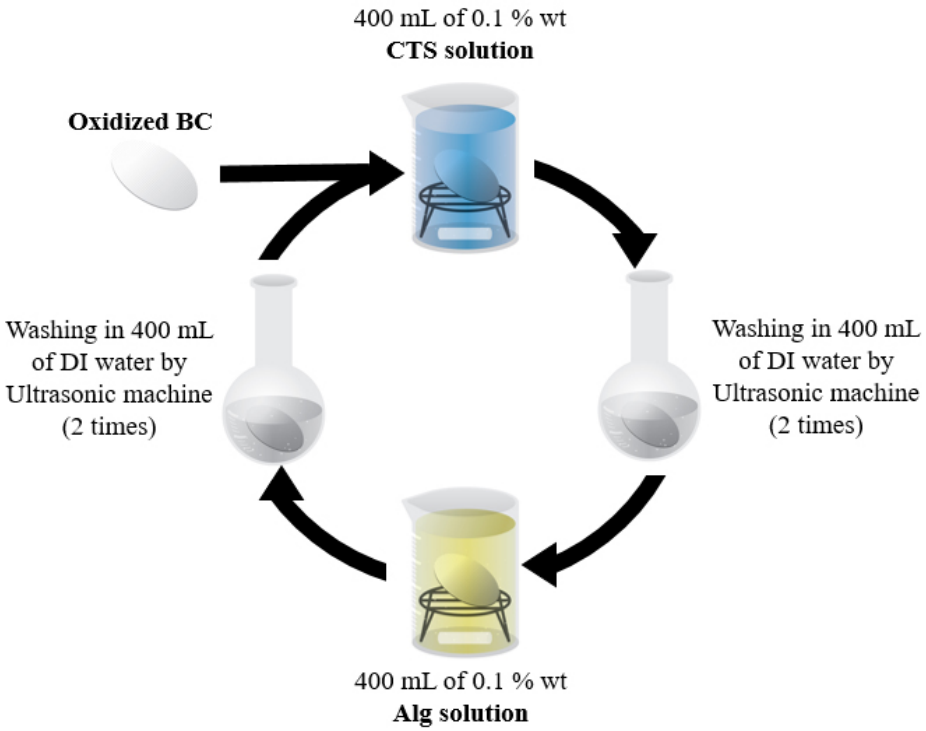

Fig. 1 A schematic diagram of the CTS/Alg coating method

Table 1 A number of the coating layer of the samples

Sample name	Number of layer	
	CTS	Alg
BC	0	0
BC(CTS/Alg)$_5$	5	5
BC(CTS/Alg)$_{10}$	10	10
BC(CTS/Alg)$_{15}$	15	15

2.2.3. Characterization of gel electrolyte

2.2.3.1. Fourier transform infrared spectroscopy (FTIR)

FTIR (FTIR; 670-IR, VARIAN Inc., USA) was used for identification of the functional groups in the obtained samples.

2.2.3.2. Determination of CTS content

The CTS content in the obtained samples was determined via the Kjeldahl method [45, 46]. The sample was dried at 50 °C overnight; then, it was vacuum dried at room temperature overnight before analysis. First, the digestion process was performed as follows: Approximately 100 mg of the sample was digested with 10 mL of concentrated sulfuric acid in the presence of 3 g of catalyst (9:1 ratio of potassium sulfate:copper sulfate) and 5 mL of 35% (v/v) hydrogen peroxide in a digestion tube at 420 °C until the digested solution became transparent. The digested solution was then cooled to room temperature, and distillation and titration were performed as follows: The digestion tube with the digestion solution was attached to the distillation unit and 30% (w/v) of NaOH solution was added to the digestion solution until the solution turned black. Steam distillation was performed for approximately 15 min. The distilled ammonia was received into DI water (30 mL) containing 2–4 mL of 0.05 M hydrochloric acid (HCl) in the Erlenmeyer flask. A few drops of the indicator (a 0.05% (w/v) methyl red-methylene blue ethanol solution) were added to the solution before titrating the solution with a standardized 0.01 M NaOH solution. The CTS content (%) was determined using equations (1) and (2):

$$M_{CTS} = M_{GlcN}\frac{DDA}{100} + M_{GlcNAc}\frac{100 - DDA}{100} \quad (1)$$

$$\text{CTS content } (\%) = \frac{M_{CTS}(C_{HCl}V_{HCl} - C_{NaOH}V_{NaOH})}{W} \times 100 \quad (2)$$

where M_{CTS} is the average molecular weight of a sugar unit of CTS and M_{GlcN} and M_{GlcNAc} are the molecular weights of a glucosamine unit and an N-acetyl-glucosamine unit, respectively. C (g/1000 mL) and V (mL) denote the concentrations and volumes of HCl and NaOH, respectively. W (g) is the total weight of the tested sample.

2.2.3.3. Scanning electron microscopy (SEM)

SEM (JSM6700, JEOL, Japan) was used for analyzing the morphology of the obtained samples and observed at an accelerating voltage of 5 kV with 20 k magnification.

The diameter-size distribution of the BC nanofibers was analyzed using image visualization software with the SEM images.

2.2.3.4. Porosity

Porosity of the sample was determined using liquid displacement according to previous literature [47]. Ethanol was used as the displacing liquid. The sample dimensions were measured using a vernier caliper, and the volume was calculated. The sample was freeze-dried and soaked in ethanol for 24 h to allow the ethanol to penetrate into the pores of the sample. The weight of the sample before and after soaking in ethanol was measured. The porosity (%) of the sample was determined using equation (3)

$$\text{Porosity (\%)} = \frac{(W_f - W_i)}{\rho_{ethanol} \times V} \times 100 \quad (3)$$

where W_f (g) is the weight of the dry sample, W_i (g) is the weight of the wet sample after soaking in ethanol, $\rho_{ethanol}$ (0.789 g/cm^3) is the density of ethanol, and V (cm^3) is the volume of the sample.

2.2.3.5. Thermogravimetric analysis (TGA)

A thermogravimetric/differential thermal analyzer (EXSTAR TG/DTA6200, SII, Japan) was used to analyze the thermal properties of the obtained samples. All samples were vacuum dried at room temperature for 2 days before analysis. The samples were measured at a heating rate of 20 °C/min in the range of 25 °C–600 °C in a nitrogen atmosphere.

2.2.3.6. Determination of mechanical properties

The mechanical properties of the obtained samples were determined using a universal testing machine (STA-1150, A&D Company, Ltd, Japan) equipped with a 50-N load cell at a constant speed of 10 mm/min in ambient conditions. The sample was cut to a size

of 30 mm in length and 5 mm in width, was mounted in tensile grips before the analysis, and was measured more than 10 times. Tensile parameters, including tensile strength and elongation at break, were determined from the stress–strain curves obtained from the force–distance data.

2.2.4. Fabrication of EDLCs cells

The BC, BC/$(CTS/Alg)_5$, BC/$(CTS/Alg)_{10}$ and BC/$(CTS/Alg)_{15}$ samples were cut into 16-mm diameter disks and immersed in $EMImBF_4$. The immersed samples were then vacuumed under 0.3 Pa at room temperature for 48 h to remove impurities such as methanol and moisture. The thicknesses of the obtained gel electrolytes were approximately 100 μm.

An activated-carbon composite electrode for a test cell was prepared via the following process. Activated carbon, acetylene black (as a conductive additive), 1.2% (w/w) sodium carboxymethyl cellulose (as a dispersant), and 48% (w/w) styrene-butadiene rubber (as a binder) were homogeneously dispersed in DI water with a weight ratio of 90:5:3:2. The obtained electrode slurry was cast onto an etched aluminum current collector and dried, and the obtained composite electrode sheet was cut into 12-mm diameter disks.

A pair of activated-carbon electrodes was immersed in $EMImBF_4$ for 10 min under a vacuum before assembling the test cells. Two-electrode coin cells were assembled using this pair of electrodes and a gel electrolyte (one of the samples described previously) for electrochemical measurements. A test cell containing $EMImBF_4$ as a liquid electrolyte with a cellulose separator (TF4035, Nippon Kodoshi Corporation, Japan) was also fabricated for comparison. All assembly procedures were conducted in an argon-filled glove box.

2.2.5. Electrochemical measurement

The performances of these EDLC test cells were measured using a battery charge–discharge apparatus (HJ1001 SM8, Hokuto Denko Corporation, Japan). The charge–discharge tests were conducted with a voltage range of 0–2.5 V at several current densities in the range of 2.5–100 mA/cm2. The discharge-rate performance of the EDLCs at various discharge current densities was also estimated after applying a constant-current charge up to 2.5 V. The discharge

capacitance of a single electrode in the present EDLC symmetrical cells was determined using equation (4):

$$C = \frac{I \times t}{(V/2) \times W} \tag{4}$$

where C (F/g) is the discharge capacitance, I (A) is the discharge current, t (s) is the discharge time, V (V) is the operating voltage, and W (g) is the mass loading of activated carbon at a single electrode [35–38]. Alternative current (AC) impedance of the test cells was measured using a potentiogalvanostat (SI 1287 type, Solartron Analytical, UK) and frequency response analyzer (SI 1260 type, Solartron Analytical, UK). The AC amplitude was 10 mVp-0 and the frequency range was 500 kHz–10 mHz. All of the electrochemical measurements were carried out at 25 °C.

2.3. Results and discussion

2.3.1. Characterization of gel electrolyte

2.3.1.1. Determination of CTS content

After coating with alternating layers of CTS and Alg, the CTS content (%) in the BC of several samples is shown in Fig. 2. The results show that the CTS content linearly increased (R^2 = 0.999) when the number of CTS layers on the BC increased, implying that the layers of CTS and Alg bound to each fiber of BC. A schematic of the coating process is shown in Fig. 3.

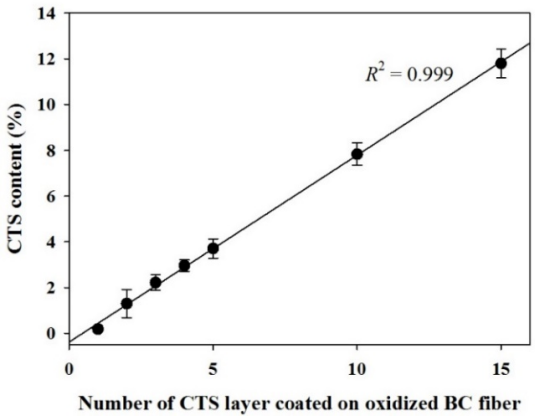

Fig. 2 CTS content in the BC coated with alternating layers of CTS and Alg

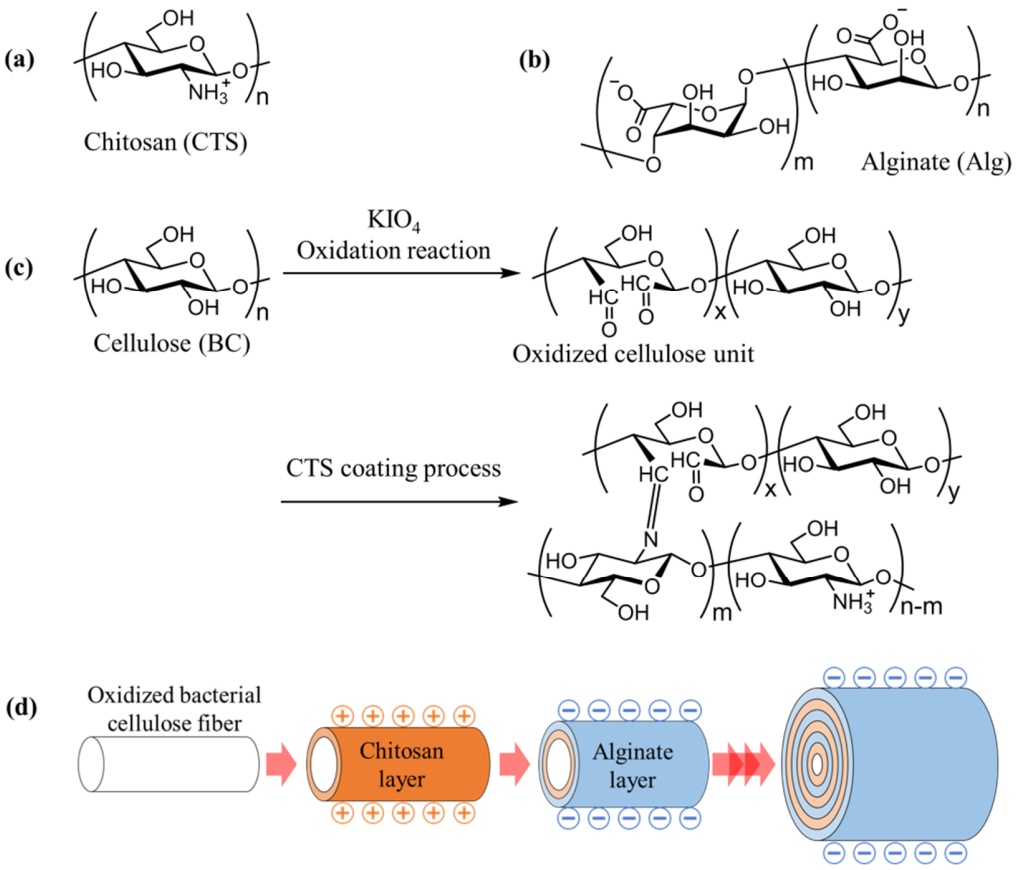

Fig. 3 Schematic of the process for coating CTS and Alg layers on BC: (a) CTS structure, (b) Alg structure, (c) cellulose oxidation reaction and CTS coating process on BC, and (d) layer-by-layer coating process with CTS and Alg

2.3.1.2. FTIR

The FTIR spectra of BC and BC coated with alternating layers of CTS and Alg are shown in Fig. 4. All samples showed absorption peaks in the region 3600 to 3000 cm^{-1}, which correspond to the stretching vibrations of O–H groups and peaks at approximately 2900 cm^{-1}, which are induced by the stretching vibration of CH_2. The various peaks in the 1450 to 1200 cm^{-1} region are due to the stretching of C–H and the peak in the region about 1060 and 1035 cm^{-1} are due to the stretching of C–O–C. These absorption peaks are characteristic of BC, while the absorption peak at 1640 cm^{-1} is related to the H–O–H bending vibration of water absorbed in the material [48, 49].

Owing to the small percentage of CTS and Alg on the BC fiber, the FTIR spectrum of BC coated alternating layers of CTS and Alg is very similar to that of the BC. However, the most obvious difference between their FTIR spectra is the slight shift of the broad peak for the O–H and N–H groups of BC/$(CTS/Alg)_5$, BC/$(CTS/Alg)_{10}$, and BC/$(CTS/Alg)_{15}$ compared with the peaks seen in normal BC in the ranges of 3370 to 3400, and 3430 to 3457 cm^{-1}, respectively. The increase in the CTS content on the BC fiber after coating with alternating layers of CTS and Alg indicates that an increased amount of amine groups or nitrogen atoms from the CTS layer were incorporated into the BC matrix and they interacted with the O–H group in the BC fiber [50]. Moreover, the peak at approximately 1420 cm^{-1} in the coated BC was stronger with a higher intensity than the same peak seen in BC because of the additional vibration from the NH_3^+ group of CTS interacting with the COO^- group of Alg [51]. Further, the peak at 1736 cm^{-1} was not found in the spectrum of the coated BC because there were no non-ionized COOH groups. These spectra confirmed that the carboxylate groups of sodium Alg were dissociated to COO^-, which formed complexes with the protonated amino groups of CTS via electrostatic interactions [52]. This result supports the measured CTS content results, which showed that CTS and Alg layers successfully bound on the BC fiber.

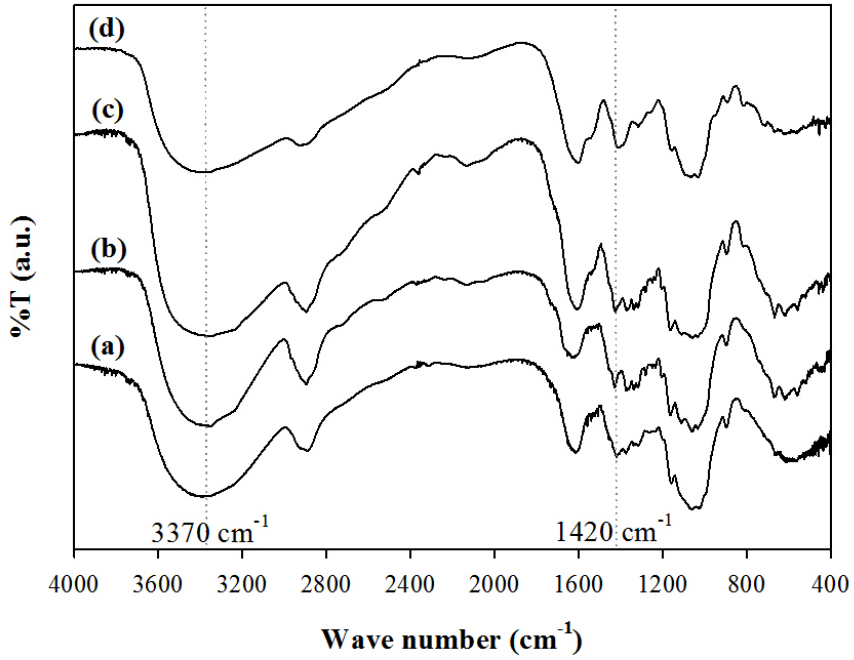

Fig. 4 Fourier transform infrared spectroscopy spectra of (a) BC, (b) BC/$(CTS/Alg)_5$, (c) BC/$(CTS/Alg)_{10}$, and (d) BC/$(CTS/Alg)_{15}$

2.3.1.3. SEM

SEM images and the measured diameter-size distribution from the SEM images of BC and coated BC are shown in Fig. 5. SEM images of BC (Fig. 5(a)) revealed a nanofibrous structure with an average fiber diameter of 76.8 nm, which is similar to the diameter reported in previous studies of BC [53, 54]. The diameter sizes of coated BC samples, BC/)CTS/Alg($_5$, BC/)CTS/Alg($_{10}$, and BC/)CTS/Alg)$_{15}$ were 78.1, 96.3, and 99.0 nm, respectively. The diameter size increased with an increase in the number of coating layers of CTS and Alg bound on each fiber of BC, which is consistent with the results of the CTS content and FTIR characterization.

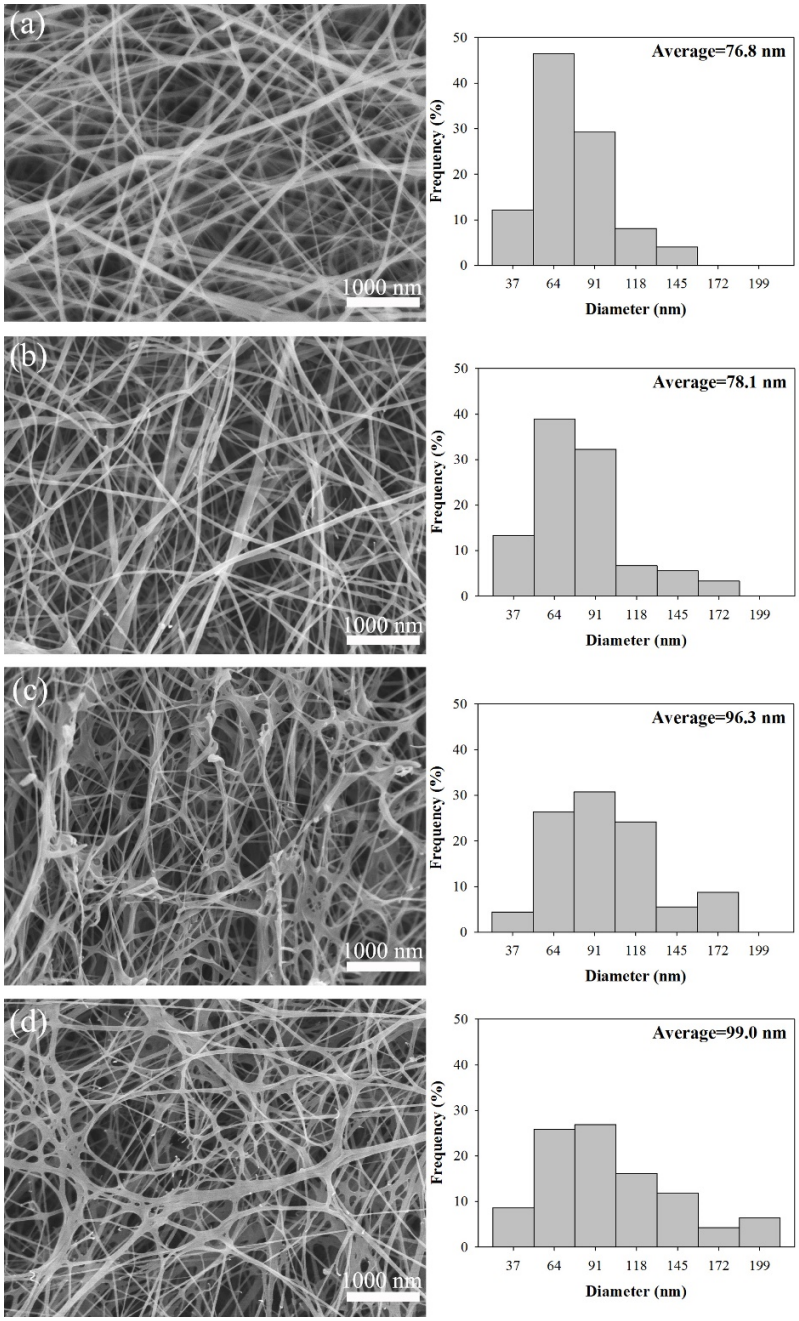

Fig. 5 Scanning electron microscopy images and the measured diameter-size distribution of (a) BC, (b) BC/$(CTS/Alg)_5$, (c) BC/$(CTS/Alg)_{10}$, and (d) BC/$(CTS/Alg)_{15}$

2.3.1.4. Porosity

The porosity at swelling stage of BC, BC/)CTS/Alg($_5$, BC/)CTS/Alg($_{10}$, and BC/)CTS/Alg)$_{15}$ were 93.5, 89.9, 88.1, and 83.3%, respectively. The porosity of the obtained samples decreased with an increase in the number of coating layers of CTS and Alg onto the BC fiber. This result suggests that the porosity of the BC gel decreased with the increase of the diameters of BC fibers which were obtained from the SEM observation.

2.3.1.5. TGA

The TGA and differential TGA (DTGA) curves of BC, coated BC, CTS powder, and sodium Alg powder are shown in Fig. 6. The CTS and sodium Alg powder had degradation temperatures at 305 °C and 240 °C due to the decomposition of CTS [55] and sodium Alg [56], respectively. BC and coated BC demonstrated a weight loss due to evaporation of the volatile content between 30 °C–130 °C; the amount of this evaporated volatile content increased in the coated BC compared to BC. The BC sample showed mere one step of degradation at approximately 360 °C owing to the dehydration and the decomposition of cellulose molecules [57, 58]. The coated BC showed two steps of degradation; the first degradation step occurred in the range of 180 °C–270 °C, which is in the same range as that of the degradation of sodium Alg and CTS, and it is therefore possible that this observation is due to the complex degradation process of Alg and CTS; the second step of degradation occurred in the range of 360 °C–380 °C, which is similar to the degradation observed in BC due to dehydration and decomposition of cellulose molecules. Therefore, the results further demonstrated that the process of coating layers of CTS and Alg on the BC fiber was successful.

In addition, all obtained samples of coated BC showed high thermal stability; therefore, this material has potential to be used as gel electrolyte in EDLCs at high operating temperatures.

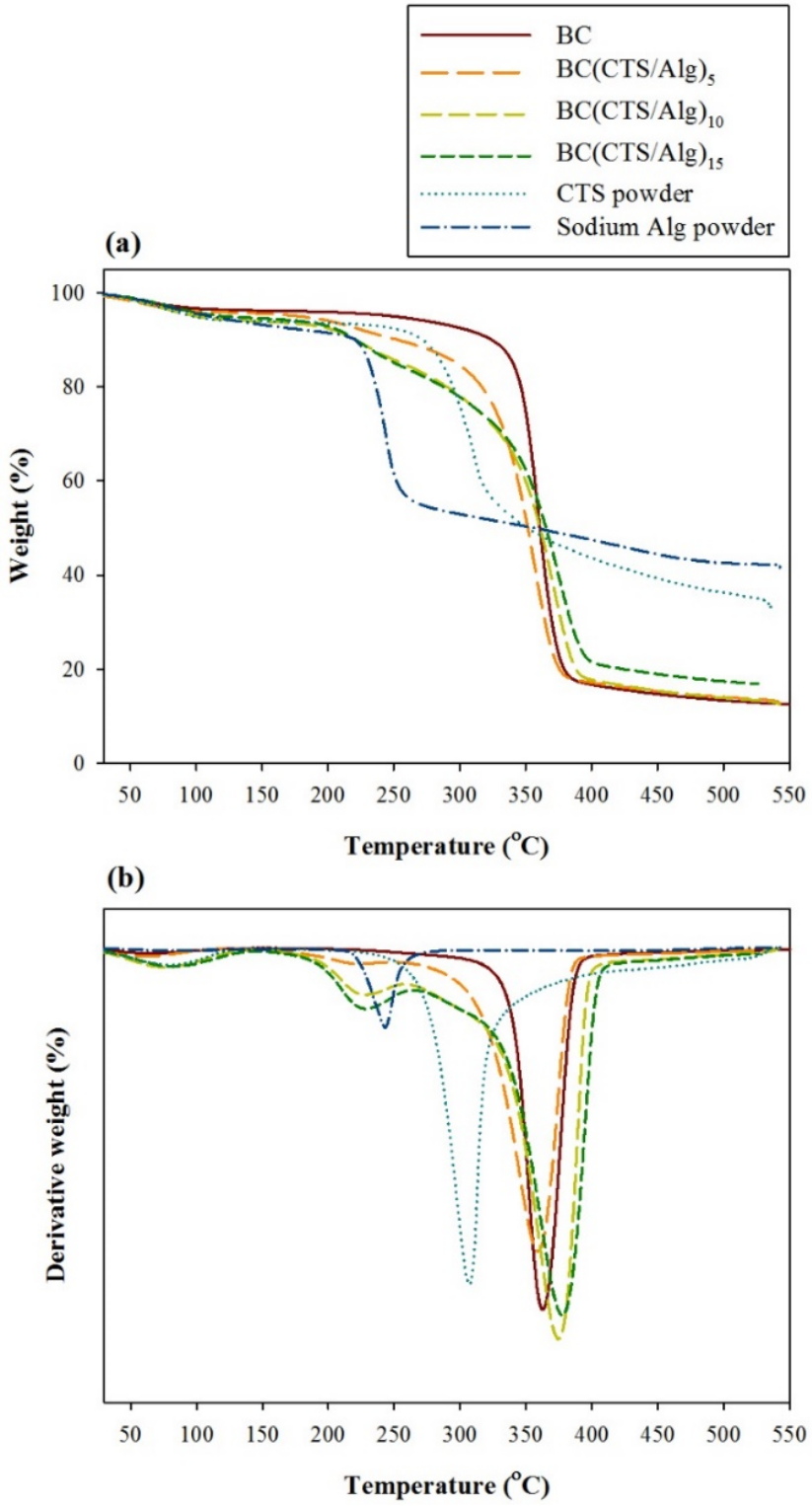

Fig. 6 (a) TGA and (b) DTGA curves of BC, BC coated with alternating layers of CTS and Alg, CTS powder, and sodium Alg powder

2.3.1.6. Mechanical properties

The mechanical properties of BC and coated BC are shown in Table 2. The CTS and Alg gel electrolytes for EDLCs were prepared for comparison of their mechanical properties [33–38]. The mechanical properties of all samples were measured at the water swelling stage. Results showed that the BC had tensile strength as high as 5.4 N, and its tensile strength increased with an increase in the number of CTS/Alg coating layers, which was possibly caused by the increasing fiber–fiber interaction within the sample. Considering the increase in fiber size that was observed with the increase in the number of CTS/Alg layers as seen in the SEM images, a decrease in the distance between fibers in a sample may cause the observed increase in the fiber–fiber interactions. Moreover, the tensile strengths of all gel electrolyte samples made with BC and coated BC were significantly higher than those of the gel electrolyte made with CTS/Alg. It should be noted that BC is used as a scaffold for the CTS and the Alg layers to improve the tensile strength of the resulting gel electrolyte.

On the contrary, the elongation at break was consistent in both the BC and the coated BC with an average elongation of approximately 42%, which is lower than that of the gel electrolyte made from CTS and Alg and which likely arises from the fibrous structure of the material.

Table 2 Tensile strength and elongation at break of various samples

Sample	Tensile strength (N)	Elongation at break (%)
BC	5.38 ± 1.09	42.21 ± 5.92
$BC(CTS/Alg)_5$	4.48 ± 0.40	52.85 ± 8.07
$BC(CTS/Alg)_{10}$	5.52 ± 0.86	33.38 ± 4.75
$BC(CTS/Alg)_{15}$	8.96 ± 2.28	39.47 ± 5.43
CTS gel	0.47 ± 0.06	72.05 ± 8.70
Alg gel	0.01 ± 0.00	38.63 ± 5.67

2.3.2. Electrochemical results

The charge–discharge curves of the EDLC test cells assembled with either the liquid-phase $EMImBF_4$ or the BC gel electrolyte with $EMImBF_4$ (BC/$EMImBF_4$) collected at current densities of 2.5 and 50 mA/cm^2 are shown in Fig. 7(a) and 7(b), respectively. During the 2.5-mA/cm^2 charge–discharge cycle, both cells showed ideal triangular charge–discharge voltage profiles, like those of typical EDLCs. On the contrary, in the charge–discharge curves measured at 50 mA/cm^2, the test cell with the BC/$EMImBF_4$ gel electrolyte showed a significantly larger IR drop than the test cell with liquid-phase $EMImBF_4$ as twice time. This result indicates that the BC/$EMImBF_4$ gel electrolyte had a higher resistance than that of the $EMImBF_4$.

To improve the rate of poor performance of the BC gel electrolyte system, the 5-, 10-, and 15-layers of the CTS and Alg coated BC gel electrolytes, including $EMImBF_4$ (BC/$(CTS/Alg)_5$/$EMImBF_4$, BC/$(CTS/Alg)_{10}$/$EMImBF_4$, and BC/$(CTS/Alg)_{15}$/$EMImBF_4$, respectively) were prepared as gel electrolytes, which had ionic functional groups with a good affinity for ionic liquids. The electrochemical performance of the electrolyte was investigated. The charge–discharge curves of the EDLC test cells assembled with the liquid-phase $EMImBF_4$, BC/$EMImBF_4$, BC/$(CTS/Alg)_5$/$EMImBF_4$, BC/$(CTS/Alg)_{10}$/$EMImBF_4$, or BC/$(CTS/Alg)_{15}$/$EMImBF_4$ collected at high current densities of 100 mA/cm^2 are shown in Fig. 6(c). The results showed that the EDLC test cells containing BC gel electrolytes with smaller numbers of CTS/Alg layers had poor electrochemical performances. The test cell with BC/$EMImBF_4$, BC/$(CTS/Alg)_5$/$EMImBF_4$, and BC/$(CTS/Alg)_{10}$/$EMImBF_4$ gel electrolyte systems showed a large IR drop than the liquid-phase $EMImBF_4$ system, while the test cells with the BC/$(CTS/Alg)_{15}$/$EMImBF_4$ gel electrolyte showed an improved small IR drop, similar to that observed in the liquid-phase $EMImBF_4$ system.

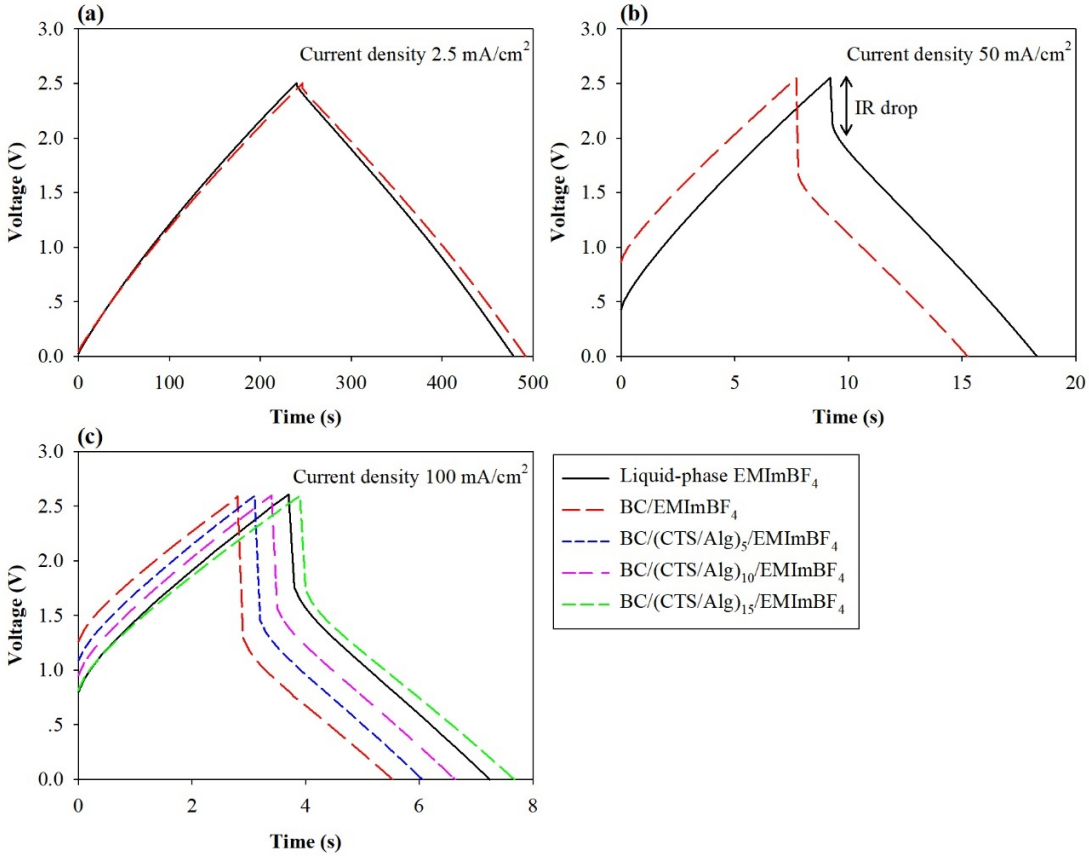

Fig. 7 Charge–discharge curves of the EDLC test cells assembled with the liquid-phase $EMImBF_4$ or the obtained gel electrolytes, collected at current densities of (a) 2.5, (b) 50 and (c) 100 mA/cm^2

In addition, the discharge capacitances of the test cells assembled with the liquid-phase $EMImBF_4$ and various gel electrolytes as a function of the applied current density (2.5–100 mA/cm^2) are shown in Fig. 8. The test cells with $BC/EMImBF_4$, $BC/(CTS/Alg)_5/EMImBF_4$, and $BC/(CTS/Alg)_{10}/EMImBF_4$ gel electrolyte showed lower discharge capacitance retention than the liquid-phase $EMImBF_4$ system, and their difference became more significant with an increase in current density, while the test cells with the $BC/(CTS/Alg)_{15}/EMImBF_4$ gel electrolyte showed a relatively higher discharge capacitance than the test cells with the liquid-phase $EMImBF_4$ system across the entire current density range. The calculated capacitance retentions from the initial current density of 2.5 to 100 mA/cm^2 of the test

cells with the liquid-phase $EMImBF_4$, $BC/EMImBF_4$, $BC/(CTS/Alg)_5/EMImBF_4$, $BC/(CTS/Alg)_{10}/EMImBF_4$, and $BC/(CTS/Alg)_{15}/EMImBF_4$ gel electrolyte were 59.6%, 45.4%, 51.2%, 55.7%, and 60.7%, respectively. The results showed that the calculated capacitance retentions of the test cell with the $BC/(CTS/Alg)_{15}/EMImBF_4$ system were slightly higher than liquid-phase $EMImBF_4$ system and were also comparable with the test cell using gel electrolyte from CTS or Alg, as shown in a previous report [34, 38], which significantly improved the tensile strength. As a result, it should be noted that the $BC/(CTS/Alg)_{15}/EMImBF_4$ was suitable and necessary to guarantee excellent electrochemical performance of the EDLC cells.

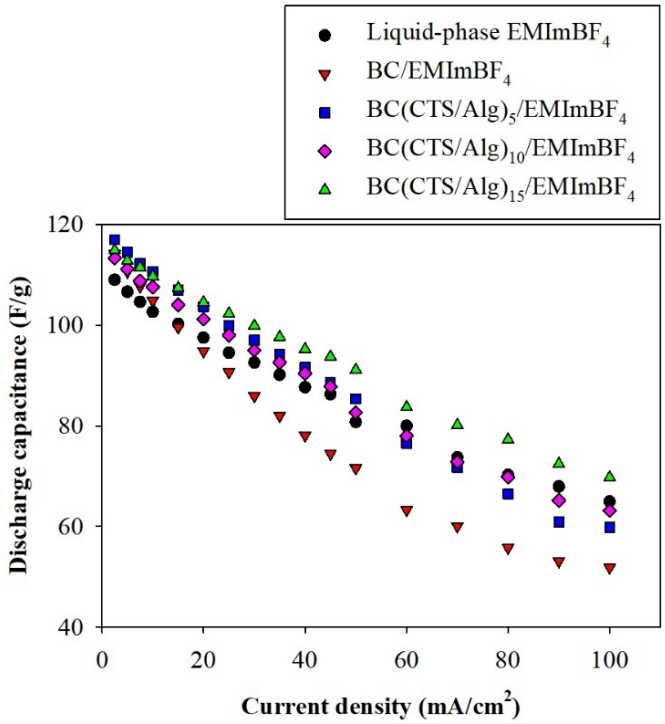

Fig. 8 Discharge capacitances of the EDLC test cells assembled with the liquid-phase $EMImBF_4$ or the obtained gel electrolytes

To investigate the role of the Alg and CTS coating on BC fiber, AC impedance was measured on the test cells. The Nyquist plots of the test cells assembled with the liquid-phase $EMImBF_4$, $BC/EMImBF_4$, and $BC/(CTS/Alg)_{15}/EMImBF_4$ gel electrolytes are shown in Fig. 9. The thicknesses of all gel electrolytes were larger than those of the separator in the liquid-

phase $EMImBF_4$ system. Nevertheless, the resistances of the electrolyte bulk, which correspond to the distance from the origin to the first intercept on the real axis, were similar for all the tested electrolyte systems (~1 Ω cm^2). Therefore, it can be concluded that the differences in rate performance do not arise from the bulk properties or thickness of the gel electrolytes. Conversely, there are considerable differences in the magnitudes of the semicircular components, which represent the contact resistance between an electrode and electrolyte [38, 59]; the observed semicircle of the test cell with $BC/EMImBF_4$ was larger than that of the test cell with liquid-phase $EMImBF_4$ by about two times, which proves the BC fiber was in poor contact with the activated carbon that lead to a large IR drop as showed in charge-discharge measurements; whereas the $BC/(CTS/Alg)_{15}/EMImBF_4$ gel electrolyte system showed a slightly smaller semicircle than that of the liquid-phase $EMImBF_4$ system due to the present surface modification of the BC fibers, which was achieved by coating with CTS and Alg layers that would facilitate better contact at the gel electrolyte/electrode interface and would accelerate ion transfer between them.

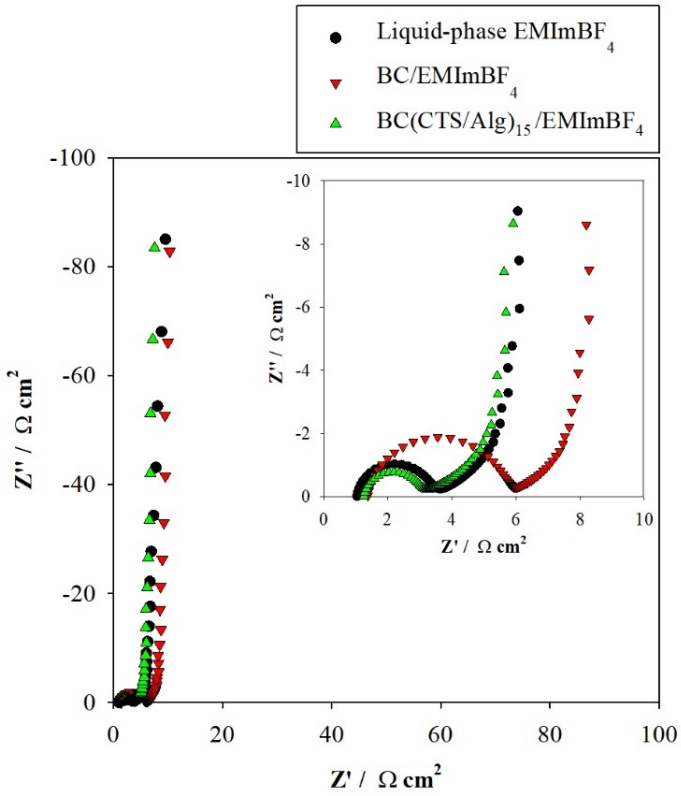

Fig. 9 Nyquist plots obtained using AC impedance measurements of the EDLC test cells assembled with the liquid-phase $EMImBF_4$, BC/$EMImBF_4$, or BC/$(CTS/Alg)_{15}$/$EMImBF_4$ gel electrolyte

2.4. Conclusions

In this study, a novel gel electrolyte was successfully prepared using BC coated with alternating layers of CTS and Alg for employing it as both an electrolyte and a separator in solid-state EDLCs. These gel electrolytes were produced via inoculation of the BC, oxidation in a KIO_4 solution, and coating with CTS layers alternated with Alg layers. Through analysis and characterization of the gel electrolytes, the CTS content linearly increased ($R^2 = 0.999$) when the number of CTS layers on the BC increased, suggesting that the layers of CTS and Alg successfully bound onto each BC fiber. The FTIR spectra of the coated BC showed a stronger peak at 1420 cm^{-1} than unmodified BC due to the vibration of NH_3^+ groups from CTS interacting with the COO^- groups of Alg. Morphological analysis from SEM images of the obtained gel electrolyte revealed a nanofibrous structure with diameter sizes of 76.8, 78.1, 96.3, and 99.0 nm , and the porosity were 93.5, 89.9, 88.1, and 83.3 % for the BC, BC/)CTS/Alg(5, BC/)CTS/Alg(10, and BC/)CTS/Alg)15 samples, respectively. The TGA and DTGA results revealed that the all obtained gel electrolytes had high thermal stabilities; the tensile measurement result showed very high tensile strengths in the coated BC samples as compared with the gel electrolytes made from raw CTS or Alg.

The electrochemical properties of EDLC test cells, which were assembled from the obtained gel electrolytes and carbon electrodes, were measured in terms of their charge–discharge characteristics, discharge capacitances, and AC impedance. The test cell with the BC/)CTS/Alg)15/$EMImBF_4$ gel electrolyte showed a comparable IR drop to the test cell with liquid-$EMImBF_4$ at switching point from charge to discharge when tested at a high current density and a higher discharge capacitance than the test cell with liquid-phase $EMImBF_4$ across the current density range, indicating that the internal resistance of the test cell decreases when the coated BC was used as the gel electrolyte. Likewise, the AC impedance results seen in the Nyquist plot of the test cell with BC/)CTS/Alg)15 represent the decrease in resistance compared with the resistance of the test cell with liquid-phase $EMImBF_4$, which verified that the high affinity of the proposed gel electrolyte for activated-carbon electrodes can reduce the charge-

transfer resistance at the electrode/electrolyte interface. The device performances demonstrate that it is possible to design simple high-operating-voltage EDLCs that can replace liquid-based electrolyte systems, and thus improve the safety of such devices.

2.5. References

[1] Y. Honda, M. Takeshige, H. Shiozaki, T. Kitamura, K. Yoshikawa, S. Chakrabati, O. Suekane, L. Pen, Y. Nakayama, M. Yamagata, M. Ishikawa, J. Power Sources 185, 1580–1584 (2008)

[2] S. Yamazaki, T. Ito, M. Yamagata, M. Ishikawa, Electrochim. Acta 86, 297–297 (2012)

[3] S. Yamazaki, K. Obata, Y. Okuhama, Y. Matsuda, M. Yamagata, M. Ishikawa, J. Power Sources 195, 1753–1756 (2010)

[4] M. Galiński, A. Lewandowski, I. Stępniak, Electrochim. Acta 51, 5567–5580 (2006)

[5] M. Tokita, N. Yoshimoto, K. Fujii, M. Morita, Electrochim. Acta 209, 210–218 (2016)

[6] R.A. Sheldon, Green Chem. 7, 267–278 (2005)

[7] F. Endres, S.Z.E. Abedin, Phys. Chem. Chem. Phys. 8, 2101–2116 (2006)

[8] N.V. Plechkova, K.R. Seddon, Chem. Soc. Rev. 37, 123–150 (2008)

[9] A. Lewandowski, M. Galiński, J. Phys. Chem. Solids 65, 281–286 (2004)

[10] Z. Zhou, M. Takeda, M. Ue, J. Fluorine Chem. 125, 471–476 (2004)

[11] T. Sato, G. Masuda, K. Takagi, Electrochim. Acta 49, 3603–3611 (2004)

[12] 12. K. Yuyama, G. Masuda, H. Yoshida, T. Sato, J. Power Sources 162, 1401–1408 (2006)

[13] C.O. Ania, J. Pernak, F. Stefaniak, E. Raymundo-Piñero, F. Béguin, Carbon 44, 3126–3130 (2006)

[14] N. Handa, T. Sugimoto, M. Yamagata, M. Kikuta, M. Kono, M. Ishikawa, J. Power Sources 185, 1585–1588 (2008)

[15] M.M. Rao, J.S. Liu, W.S. Li, Y. Liang, D.Y. Zhou, J. Membr. Sci. 322, 314–319 (2008)

[16] B. Rupp, M. Schmuck, A. Balducci, M. Winter, W. Kern, Eur. Polym. J. 44, 2986–2990 (2008)

[17] M. Rao, X. Geng, Y. Liao, S. Hu, W. Li, J. Membr. Sci. 399-400, 37–42 (2012)

[18] R. Prasanth, N. Shubha, H.H. Hng, M. Srinivasan, Eur. Polym. J. 49, 307–318 (2013)

[19] K. Karuppasamy, P.A. Reddy, G. Srinivas, A. Tewari, R. Sharma, X.S. Shajan, D. Gupta, J. Membr. Sci. 514, 350–357 (2016)

[20] P.F.R. Ortega, J.P.C. Trigueiro, G.G. Silva, R.L. Lavall, Electrochim. Acta 188, 809–817 (2016)

[21] M. Safa, A. Chamaani, N. Chawla, B. El-Zahab, Electrochim. Acta 213, 587–593 (2016)

[22] J. Rymarczyk, M. Carewska, G.B. Appetecchi, D. Zane, F. Alessandrini, S. Passerini, Eur. Polym. J. 44, 2153–2161 (2008)

[23] N.N. Mobarak, N. Ramli, A. Ahmad, M.Y.A. Rahman, Solid State Ionics 224, 51–57 (2012)

[24] N.N. Mobarak, F.N. Jumaah, M.A. Ghani, M.P. Abdullah, A. Ahmad, Electrochim. Acta 175, 224–231 (2015)

[25] S. Rudhziah, M.S.A. Rani, A. Ahmad, N.S. Mohamed, H. Kaddami, Ind. Crops Prod. 72, 133–141 (2015)

[26] T.M.D. Palma, F. Migliardini, D. Caputo, P. Corbo, Carbohydr. Polym. 157, 122–127 (2017)

[27] E. Rapharl, C.O. Avellaneda, B. Manzolli, A. Pawlicka, Electrochim. Acta 55, 1455–1459 (2010)

[28] R. Leones, F. Sentanin, L.C. Rodrigues, I.M. Marrucho, J.M.S.S. Esperança, A. Pawlicka, M.M. Silva, Express Polym. Lett. 6(12), 1007–1016 (2012)

[29] A.S.A. Khiar, A.K. Arof, Ionics 16, 123–129 (2010)

[30] M. Kumar, T. Tiwari, N. Srivastava, Carbohydr. Polym. 88, 54–60 (2012)

[31] M.F. Shukur, R. Ithnin, M.F.Z. Kadir, Electrochim. Acta 136, 204–216 (2014)

[32] Y.N. Sudhakar, M. Selvakumar, D. K. Bhat, Mater. Sci. Eng., B 180, 12–19 (2014)

[33] K. Soeda, M. Yamagata, S. Yamazaki, M. Ishikawa, Electrochemistry 81(10), 867–872 (2013)

[34] M. Yamagata, K. Soeda, S. Ikebe, S. Yamazaki, M. Ishikawa, Electrochim. Acta 100, 275–280 (2013)

[35] M.Yamagata, K. Soeda, S. Ikebe, S. Yamazaki, M. Ishikawa, J. Electrochem. Soc. 41(22), 25–34 (2012)

[36] M. Yamagata, K. Soeda, S. Yamazaki, M. Ishikawa, J. Electrochem. Soc. 25(35), 193–200 (2010)

[37] M. Yamagata, S. Ikebe, Y. Kasai, K. Soeda, M. Ishikawa, J. Electrochem. Soc. 50(43), 27–36 (2013)
[38] K. Soeda, M. Yamagata, M. Ishikawa, J. Power Sources 280, 565–572 (2015)
[39] Z. Wan, L. Wang, X. Yang, J. Guo, S. Yin, Food Hydrocoll. 61, 269–276 (2016)
[40] M.H. Kwak, J.E. Kim, J. Go, E.K. Koh, S.H. Song, H.J. Son, H.S. Kim, Y.H. Yun, Y.J. Jung, D.Y. Hwang, Carbohydr. Polym. 122, 387–398 (2015)
[41] S. Hestrin, M. Schramm, Biochem. J. 58, 345–352 (1954)
[42] J.K. Park, J.Y. Jung, Y.H. Park, Biotechnol. Lett. 25, 2055–2059 (2003)
[43] J.H. Kim, S. Park, H. Kim, H.J. Kim, Y. Yang, Y.H. Kim, S. Jung, E. Kan, S.H. Lee, Carbohydr. Polym. 157, 137–145 (2017)
[44] X.D. Liu, N. Nishi, S. Tokura, N. Sakairi, Carbohydr. Polym. 44, 233–238 (2001)
[45] J. Junsomboon, J. Jakmunee, Anal. Chim. Acta 627, 232–238 (2008)
[46] P. Campins-Falco, S. Meseguer-Lloret, T. Climent-Santamaria, C. Molins-Legua, Talanta 75, 1123–1126 (2008)
[47] B.S. Anisha, D. Sankar, A. Mohandas, K.P. Chennazhi, S.V. Nair, R. Jayakumar, Carbohydr. Polym. 92, 1470–1476 (2013)
[48] G. Bali, M.B. Foston, H.M. O'Neill, B.R. Evans, J. He, A.J. Ragauskas, Carbohydr. Res. 374, 82–88 (2013)
[49] M. Ul-Islam, J.H. Ha, T. Khan, J.K. Park, Carbohydr. Polym. 92, 360–366 (2013)
[50] C. Liu, R. Bai, J. Membr. Sci. 267, 68–77 (2005)
[51] W.S.W. Ngah, S. Fatinathan, Chem. Eng. J. 143, 62–72 (2008)
[52] B. Smitha, S. Sridhar, A.A. Khan, Eur. Polym. J. 41, 1859–1866 (2005)
[53] M.L. Cacicedo, M.C. Castro, I. Servetas, L. Bosnea, K. Boura, P. Tsafrakidou, A. Dima, A. Terpou, A. Koutinas, G. R. Castro, Bioresour. Technol. 213, 172–180 (2016)
[54] X. Fan, Y. Gao, W. He, H. Hu, M. Tian, K. Wang, S. Pan, Carbohydr. Polym. 151, 1068–1072 (2016)
[55] I. Corazzari, R. Nistico, F. Turci, M.G. Faga, F. Franzoso, S. Tabasso, G. Magnacca, Polym. Degrad. Stab. 112, 1–9 (2015)
[56] S. Liu, Y. Li, L. Li, Carbohydr. Polym. 160, 62–70 (2017)
[57] X. Lu, X. Shen, Carbohydr. Polym. 86, 239–244 (2011)

[58] J.A. Marins, B.G. Soares, H.S. Barud, S.J.L. Ribeiro, Mater. Sci. Eng., C 33, 3994–4001 (2013)

[59] A. Lewandowski, A. Świderska, Solid State Ionics 161, 243–249 (2003)

Chapter 3

Preparation and Characterization of Thin-film Electrolyte from Chitosan.

3.1. Introduction

Electric double-layer capacitors (EDLCs), also known as super capacitors or ultracapacitors, are electrochemical devices that have received much attention in recent years because of their outstanding properties of long cycle lifetime and high sustained power density [1–3]. Likewise, electrolytes based on natural polymers have been developed vigorously for electric devices because of their biodegradation properties, low cost, non-toxicity, environmental friendliness, richness in nature, and capacity to satisfy sustainable biopolymer development. Many natural polymers have been used as polymer electrolytes, such as alginate [4–6], carrageen [7, 8], agar [9, 10], starch [11–13], natural rubber [14, 15], pectin [16], cellulose [17], and chitosan (CS) [18–20], the last of which is one of the most abundant biomaterials.

CS is a cationic biopolymer obtained from either fully or partially deacetylated chitin. As a natural polymer, CS is a copolymer of D-glucosamine and *N*-acetyl-D-glucosamine connected via β (1-4) linkage and is present in crustacean shells, insect exoskeletons, and cell walls of some fungi [21–26]. CS is often identified by its degree of deacetylation (DDA), namely, the ratio of D-glucosamine to *N*-acetyl-D-glucosamine. The DDA is typically in the range of 70%–100% and relates to CS properties such as its surface energy, crystallinity and degradation [27, 28]. Because of its excellent biodegradability, biocompatibility, hemostasis, and antimicrobial activity and the fact that it is easily processed into various forms (e.g., hydrogels, membranes, scaffolds, beads, sponges, nanofibers, and nanoparticles), CS is extremely valuable for biomedical and pharmaceutical applications [29]. Furthermore, many studies have reported that CS is a promising electrolyte for EDLCs in terms of giving their high operating performance [30–33].

Often referred to as green solvents [34–36], ionic liquids (ILs) are organic salts whose melting points are near room temperature. One such IL is 1-ethyl-3-methylimidazolium tetrafluoroborate ($EMImBF_4$). With its high ionic conductivity and low viscosity, $EMImBF_4$ is widely used as an electrolyte in EDLCs [37–42]. In addition, ILs exhibit unique physicochemical properties such as near-zero vapor pressure, high chemical and thermal stabilities, and the facts that they remain liquid over a broad temperature range and are good at dissolving a variety of organic and inorganic compounds [34–36]. As such, ILs have been studied recently for their

abilities to dissolve native polysaccharides and some natural materials [35, 36, 43–48] including CS [49–55].

Previously, Yamagata et al. [30, 31] prepared gel electrolytes from CS including ILs via hydrogel preparation methods for use in EDLCs. Although the method provided gel electrolytes with high performance despite the use of gel electrolytes, it adversely resulted in low tensile strength, which is a favorable property for solid-electrolytes to be used in EDLCs. This failed to approximately control the IL content in the obtained sample. Thus, development on a novel method to overcome these disadvantages is desirable.

The aim of this chapter is to propose a new method to provide an IL-based thin-film electrolyte (TFE) with relatively high tensile property and appropriate IL-content. In addition, the novel CS-TEFs were used as a solid electrolyte for EDLCs to improve their safety and performance. To the best of our knowledge, this study is the first report on preparation of TFEs by using CS dissolved in the mixture of $EMImBF_4$ and water (see CS and $EMImBF_4$ structure in Fig. 1). $EMImBF_4$ in this system plays important roles as both a dissolving solution and a charge carrier for EDLC due to high ionic conductivity and low viscosity. The obtained TFE is characterized, and the electrochemical properties of an EDLC test cell containing the electrolyte were assessed.

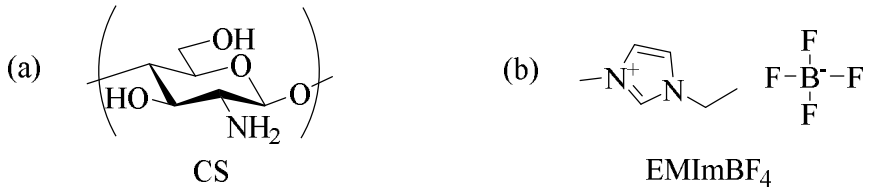

Fig. 1 Structure of (a) CS and (b) $EMImBF_4$.

3.2. Materials and methods

3.2.1. Materials

Chitosan (CS; FM-80, DDA 88.3%, Viscosity 30 mPa S, Mw 24.8×10^4) was supplied by Koyo Chemical Company (Japan), and 1-ethyl-3-methylimidazolium

tetrafluoroborate ($EMImBF_4$, 99.0%) was purchased from Toyo Gosei Company (Japan). The number average molecular weight (Mw) of CS was re-measured by gel permeation chromatography (GPC) method.

3.2.2. Preparation of CS-TFEs

CS powder was dispersed in a mixture of $EMImBF_4$ and deionized (DI) water in a glass bottle with different stoichiometric ratios as listed in Table 1, and the calculated $EMImBF_4$ in dry film was calculated according to Eq. (1). The mixture was stirred at 40°C for four days and then left at room temperature for 10 days. The obtained solution was cast into a frame made with a glass supporter (thickness; 1200-μm) on a Teflon sheet and was soaked in methanol for 3 min. The CS-TFE was then dried at 25°C (room temperature) for 24 h, then the dry sample was kept in a desiccator filled with silica-gel desiccants before being used in further steps.

$$\text{Calculated EM Im BF}_4\text{ in dry film [\%wt]} = \left(\frac{W_2}{W_1 + W_2} \right) \times 100, \quad (1)$$

where W_1 is the weight (in g) of CS and W_2 is the weight (in g) of $EMImBF_4$.

Table 1. Composition of CS solution for CS-TFEs.

Sample	Weight of CS [g]	Weight of water [g]	Weight of $EMImBF_4$ [g]	Calculated $EMImBF_4$ in dry film [wt%]
CS-BF_4-60	0.36	13.64	0.54	60
CS-BF_4-70			0.85	70
CS-BF_4-80			1.47	80

3.2.3. Characterization of CS-TFEs

3.2.3.1. Scanning electron microscopy (SEM)

The structural morphology of each sample was observed using a scanning electron microscope (SEM; JSM6700, JEOL, Japan) at an accelerating voltage of 5 kV and a magnification of 5,000.

3.2.3.2. Fourier transform infrared spectroscopy (FTIR)

The functional groups of each sample were characterized using a Fourier-transform infrared (FT-IR) spectrometer (FT/IR-4200, JASCO, Japan) via the KBr-pellet method in the wavenumber range of 400–4000 cm^{-1}.

3.2.3.3. Thermogravimetric analysis (TGA)

The thermal decomposition of each sample was tested under a nitrogen atmosphere using a thermogravimetric analyzer (TGA; EXSTAR TG/DTA6200, SII, Japan). The sample was heated from 30°C to 550°C at a heating rate of 20°C/min.

3.2.3.4. Determination of mechanical properties

The mechanical properties of each sample were determined in ambient conditions using a universal testing machine)STA-1150, A&D Company, Ltd., Japan(equipped with a 50-N load cell and operating at a constant speed of 10 mm/min. Before the analysis, the sample was cut to be 30 mm long and 5 mm wide and was mounted in tensile grips spaced 10 mm apart. The measurement was repeated more than 10 times. The tensile parameters of tensile strength and elongation at break were determined from the stress–strain curves obtained from the force–distance data.

3.2.3.5. Determination of $EMImBF_4$ content

The amount of $EMImBF_4$ in an obtained sample was determined as follows. The sample was weighed, soaked in excess dichloromethane for 24 h to remove $EMImBF_4$, dried at 60°C for 24 h, and then weighed again. This procedure was repeated until the sample weighed the same before and after the $EMImBF_4$-removal step. A percentage of the total $EMImBF_4$ content was calculated according to Eq. (2).

$$\%\ \mathrm{EMImBF_4\ content} = \left(\frac{M_1 - M_2}{M_1} \right) \times 100\,, \tag{2}$$

where M_1 is the weight (in mg) of the $EMImBF_4$-bearing sample and M_2 is the constant weight (in mg) of the sample after removing $EMImBF_4$.

3.2.4. Fabrication of EDLCs cells

Each obtained TFE was cut into a 16-mm-diameter disk and soaked in $EMImBF_4$ under 0.3-Pa vacuum at room temperature for 48 h before being assembled in the EDLC test cell. The test cell was assembled by sandwiching the TFE between two carbon electrodes in a coin-cell (CR2032, stainless type, Hohsen Corporation, Japan) in an argon-filled glove box. In addition, a test cell was assembled with liquid-phase $EMImBF_4$ with a cellulose separator (TF4035, Nippon Kodoshi Corporation, Japan) for comparison.

The symmetrical carbon electrodes were prepared by coating as follows. Activated carbon (YP-50F, specific surface area: 1500–1800 m^2/g, Kuraray Co., Ltd., Japan), acetylene black (HS-100, Denka Co., Ltd., Japan) as a conductive additive, 1.2 wt% sodium carboxymethyl cellulose (WS-C, DKS Co., Ltd., Japan) as a dispersant, and 48 wt% styrene–butadiene rubber (TRD2001, JSR Corporation, Japan) as a binder were mixed in DI water at a weight ratio of 90:5:3:2. The mixture was stirred until a homogenous slurry with a smooth surface was obtained. The obtained electrode slurry was coated on an aluminum current collector to produce a carbon electrode. The obtained carbon electrode was dried in an oven at 100°C for 10 h to eliminate the solvent and was then cut into a 12-mm-diameter disk before being used in the next steps.

3.2.5. Electrochemical measurement

The electrochemical properties of each EDLC test cell were determined in terms of its charge–discharge performance, discharge capacitance, and alternating-current (AC) impedance. The charge–discharge performance was measured using a battery charge/discharge apparatus (HJ1001 SM8, Hokuto Denko Corporation, Japan) at voltages of 0–2.5 V and various current densities. The discharge rate was estimated at discharge current densities between 2.5–100 mA/cm^2. The discharge capacitance of a single electrode in the symmetrical EDLC cell was determined using Eq. (3) [30, 31]:

$$C = \left(\frac{I \times t}{(V/2) \times W} \right) \tag{3}$$

where C is the discharge capacitance, I is the discharge current [A], t is the discharge time [s], V is the operating voltage, and W is the total mass of activated carbon in a single electrode [g].

The AC impedance was measured using a potentiogalvanostat (SI 1287, Solartron Analytical, UK) and a frequency-response analyzer (SI 1260, Solartron Analytical, UK) with an AC amplitude of 10 $mV_{p\text{-}0}$ in the frequency range of 500 kHz–10 mHz. All electrochemical measurements were performed at 25°C.

3.3. Results and discussion

3.3.1. Preparation of CS-TFEs

CS is difficult to dissolve in commonly used solvents because it has strong hydrogen bonding and a combination of amorphous and crystalline regions. Therefore, for preparing the CS electrolytes (CS-gel) in the previous reports, CS powder was dissolved in aqueous acetic acid and the solution was cast to produce the films, later soaking it in IL [30–31]. In this study, we proposed a new method to prepare CS-TFE. CS was dissolved in a mixture of $EMImBF_4$ and water that could approximately control IL content in obtained product by one-pot synthesis, and $EMImBF_4$ acts as not only the solvent for the CS but also the charge carrier for the EDLCs.

3.3.2. Characterization of CS-TFEs

3.3.2.1. SEM

SEM images of the surfaces and cross-sectional areas of the CS-TFE products are shown in Fig. 2. None of the surfaces show phase separation between the CS and $EMImBF_4$. By contrast, the surface morphology of the sample was influenced by the amount of $EMImBF_4$ in the dry film. CS-BF_4-60 (see Fig. 2(a)) had a grainy structure with unevenly distributed spots, suggesting that there was insufficient $EMImBF_4$ in the mixture solution to incorporate it into the CS matrix for complete dissolution. CS-BF_4-80 (see Fig. 2(c)) had a rough surface with a porous structure because of the low wt% of CS and high wt% of $EMImBF_4$ when the film was prepared. Moreover, the cross-sectional morphology of each sample was considered and showed that porosity was present throughout. The porosity size increased with the wt% of $EMImBF_4$ in the dry film, which could be related to the amount of CS and EMImBF4 in the mixture solution before the film was prepared.

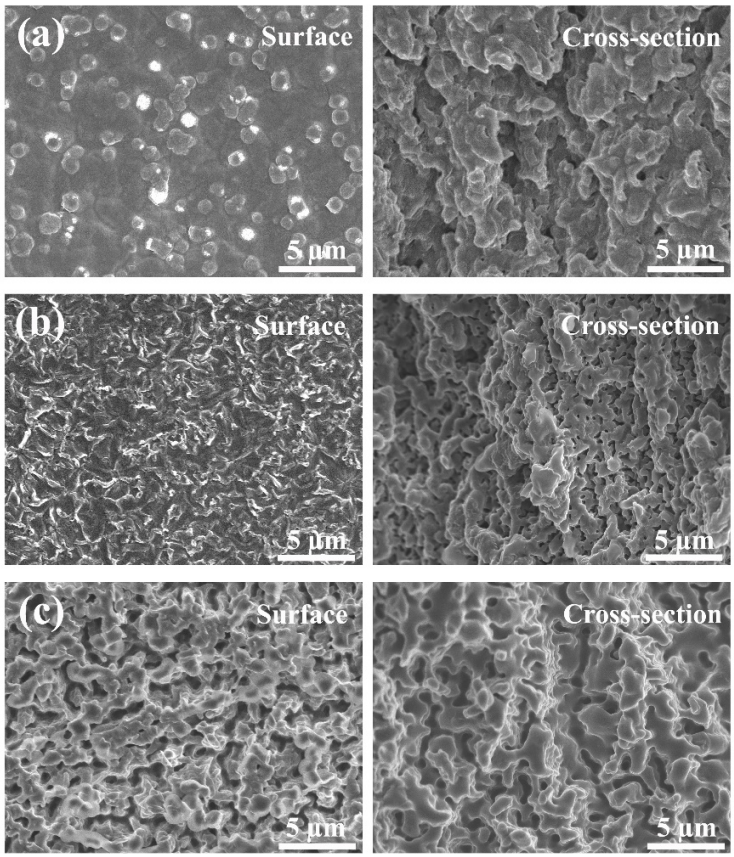

Fig. 2 SEM images of the surface and cross-sectional area of (a) CS-BF_4-60, (b) CS-BF_4-70, and (c) CS-BF_4-80.

3.3.2.2. FTIR

The FT-IR spectra of $EMImBF_4$, CS powder, and CS-TFE products are shown in Fig. 3. The adsorption peak for the CS powder is similar to that of the CS-TFE products at characteristic peaks of CS as follows. The broad band around 3,450 cm^{-1} is due to the stretching vibrations of the $–NH_2$ and –OH groups. The broad bands at 2,920 and 2,860 cm^{-1} are due to the asymmetric stretching vibrations of C–H in the sugar residue. The peak around 1,690 cm^{-1} is due to the stretching of amide I. The peaks at 1,420, 1,380, and 1,320 cm^{-1} are due to CH_2 deformation, $–CH_3$ symmetric deformation, and amide III/CH_2 wagging, respectively [22, 56, 57]. By contrast, the characteristic peaks of $EMImBF_4$ were observed on the CS-TFE products only. The new peaks at 3,140 and 2,980 cm^{-1} are due to the aliphatic asymmetric and symmetric (C–H) stretching vibrations of the imidazolium ring. The new strong peak at 1,570

cm^{-1} is due to the C=C stretching vibration of the imidazolium ring. The increased adsorption peak at 1,169 cm^{-1} is due to the C–N stretching vibration of the imidazolium ring; in particular, the peak at 1,049 cm^{-1} corresponds to the asymmetric vibrations of B–F bond [58–60]. The FT-IR spectra confirm that $EMImBF_4$ was introduced effectively into the CS-TFE products.

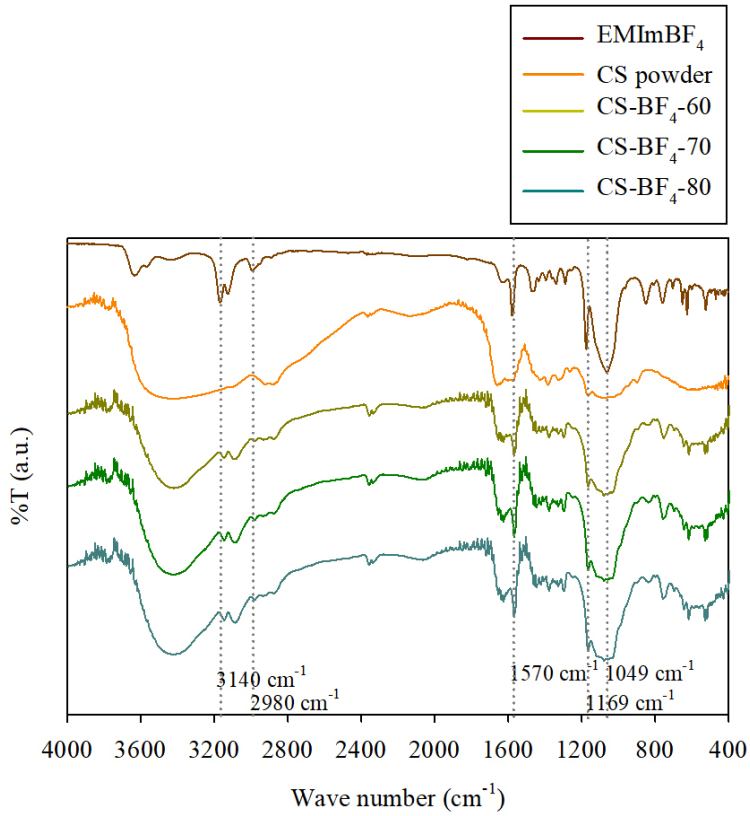

Fig. 3 FT-IR spectra of $EMImBF_4$, CS powder, and CS-TFE products.

3.3.2.3. TGA

The TGA and differential TGA (DTGA) curves of $EMImBF_4$, CS powder and CS-TFEs products are shown in Figs. 4(a) and (b), respectively. The TGA thermograms show how the sample weight decreased during thermal decomposition, and the DTGA curves show clearly the maximum decomposition temperature at each step of thermal decomposition. The CS powder and all of the CS-TFE products lost weight at temperatures of approximately 30°C –130°C because of the evaporation of volatile content. The CS powder showed only one

thermal degradation step as obtained from the peak in the DTGA curve at 307°C corresponding to the chemical degradation and deacetylation of CS molecules [61]. By contrast, the CS-TFE products showed two distinctive thermal degradation stages. The first stage was observed at around 275°C, which is near the degradation temperature observed for the CS powder and could be due to CS decomposition. The second-stage degradation temperatures of CS-TFE products CS-BF_4-60, CS-BF_4-70, and CS-BF_4-80 were 421°C, 423°C, and 437°C, respectively. The degradation temperature increased with the $EMImBF_4$ content in the dry thin film, which is attributed mainly to the decomposition of $EMImBF_4$ [62, 63]; this can be seen also in the TGA and DTGA results for pure $EMImBF_4$. Therefore, it was shown that $EMImBF_4$ was incorporated successfully into the CS-TFEs.

Furthermore, all of the CS-TFE products showed high thermal stability. Therefore, this novel material has practical potential for use as electrolyte in EDLCs operating at high temperature.

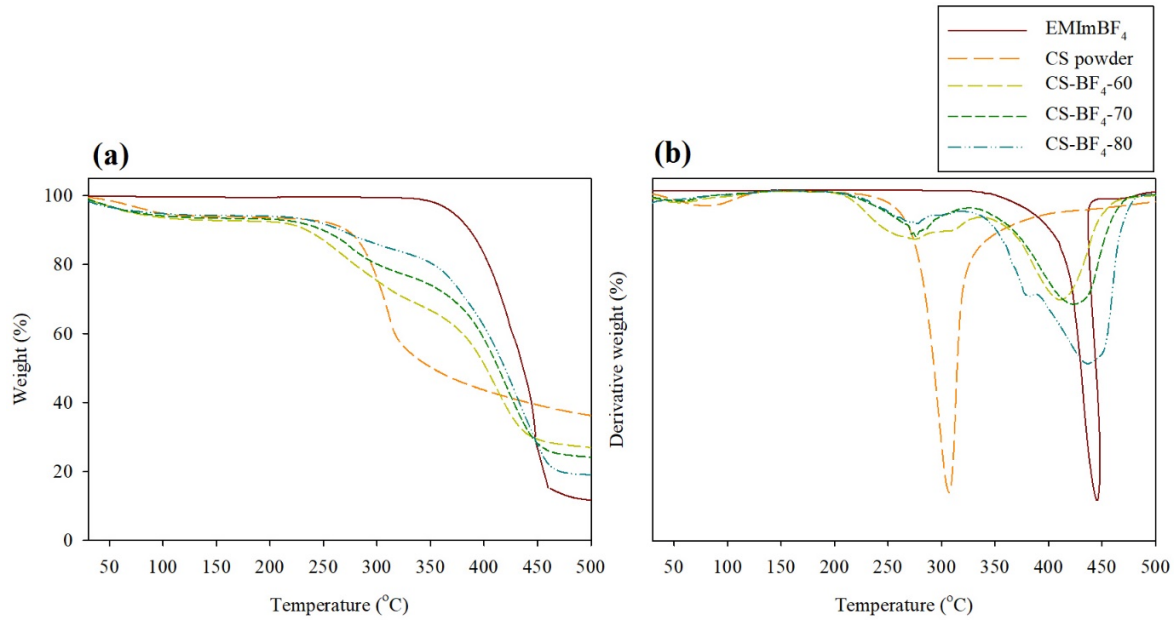

Fig. 4 (a) TGA and (b) DTGA curves of $EMImBF_4$, CS powder and CS-TFE products.

3.3.2.4. Mechanical properties

The tensile strength and elongation at break of the CS-TFE products are summarized in Table 2. Moreover, CS-gel from previous studies was replicated to compare their

mechanical properties [30–31]. The tensile strength of a sample is the maximum tensile stress sustained during tensile testing. The tensile strength decreased with the wt% $EMImBF_4$ in the dry thin film because of the decrease of the CS mass and the porous structure of the sample. However, the lowest tensile strength of the thin-film samples (that of CS-BF_4-80) was significantly higher than those of all of CS-gel samples. The elongation at break of the CS-TFE products slightly improved compare to CS-gel from 33.44% to the range of 35.02%–36.94%. The experimental results suggest that the CS-TFE product from the new preparation method exhibited improved tensile properties compared to the CS-gel systems due to the different preparation method. The viscosity of the cast solution of chitosan was higher in the present system than that in the CS-gel system, thus more dense film was prepared.

3.3.2.5. Determination of $EMImBF_4$ content

The remaining amount of $EMImBF_4$ incorporated into the CS matrix from CS-TFE preparation process of CS-BF_4-60, CS-BF_4-70, and CS-BF_4-80 were 48.05%, 53.98%, and 70.21%, respectively. The $EMImBF_4$ content of the obtained samples increased with the wt% of $EMImBF_4$ in the mixture solution used for film preparation. This result proves that this new CS-TFE preparation method is able to approximately control IL content in obtained product by one-pot synthesis. Moreover, the obtained CS-TFE was soaked in $EMImBF_4$ solution before fabrication of the EDLC test cell. The $EMImBF_4$ content of CS-BF_4-60, CS-BF_4-70, and CS-BF_4-80 were increased to 51.1%, 58.0%, and 78.8%, respectively. The $EMImBF_4$ content of CS-BF_4-80 was significantly increased as compared with those of CS-BF_4-60 and CS-BF_4-70 because of the broad porous structure of the sample as obtained from the SEM observations: the film possibly adsorbed more $EMImBF_4$ after the sample was soaked in $EMImBF_4$.

3.3.3. Electrochemical results

The obtained CS-TFEs or liquid-phase $EMImBF_4$ with a cellulose separator were assembled in EDLC test cells as electrolytes to test their electrochemical properties regarding charge–discharge performance, discharge capacitance, and Nyquist plots obtained by AC impedance measurements.

The charge–discharge curves of the EDLC test cells assembled with either liquid-phase $EMImBF_4$ or the obtained CS-TFEs are shown in Figs. 5(a), (b), and (c) for current densities of 2.5, 50, and 100 mA/cm^2, respectively. During the 2.5-mA/cm^2 charge–discharge measurements, all test cells showed a perfectly triangular shape that is a typical shape of the ideal EDLCs. In the charge–discharge curves measured at high current densities of 50 and 100 mA/cm^2, rapid voltage drops during switching (known as *IR* drops and indicated by arrow in Fig. 5(b)) occurred in all the test cells, showing a clearly larger *IR* drop with higher current density. However, the *IR* drop was reduced in the CS-TFEs with higher $EMImBF_4$ content. The CS-BF_4-60 and CS-BF_4-70 test cells showed larger *IR* drops than that of the test cell with liquid-phase $EMImBF_4$, whereas the CS-BF_4-80 test cell showed an *IR* drop that was comparable with that of the liquid-phase $EMImBF_4$ system; that may be because the ionic conductivity and internal resistance of the test cell were improved by increasing the $EMImBF_4$ content in the TFEs.

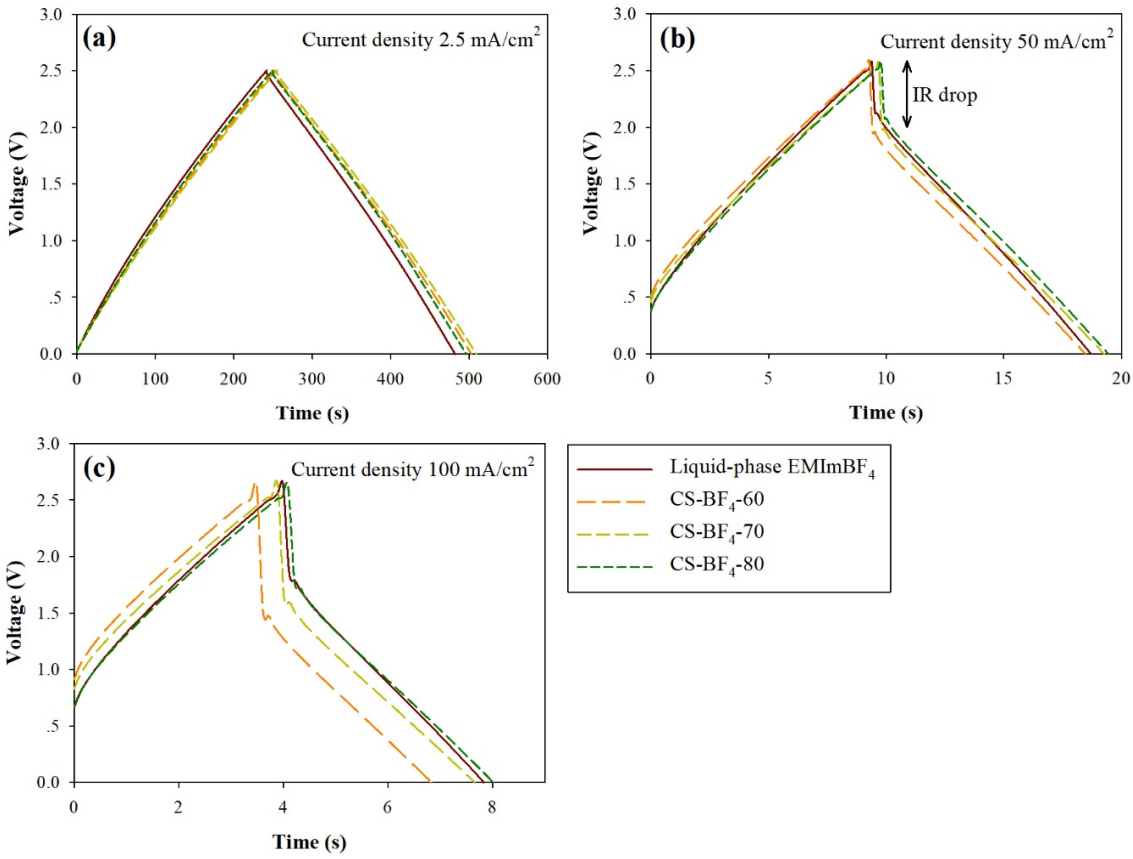

Fig. 5 Charge–discharge curves of the EDLC test cell assembled with liquid-phase $EMImBF_4$ or the obtained CS-TFEs at current densities of (a) 2.5, (b) 50, and (c) 100 mA/cm^2.

Furthermore, the discharge capacitances of the same EDLC test cells are shown in Fig. 6 as functions of the applied current density in the range 2.5–100 mA/cm^2. At low current density, the CS-BF_4-60 and CS-BF_4-70 test cells showed higher discharge capacitances compared to the liquid-phase $EMImBF_4$ test cell, becoming lower at higher current density. By contrast, the discharge capacitance of the CS-BF_4-80 test cell was higher compared to the liquid-phase $EMImBF_4$ system over the entire range of current density. Moreover, the capacitance retentions of the test cells were calculated for 2.5–100 mA/cm^2. Those of the CS-BF_4-60, CS-BF_4-70, CS-BF_4-80, and liquid-phase $EMImBF_4$ test cells were 54%, 59%, 64%, and 64%, respectively, suggesting that the capacitance retention increased with the $EMImBF_4$ content in the CS-TFEs in the TFE system; the capacitance retention of the CS-BF_4-80 test cell was comparable to that of the liquid-phase $EMImBF_4$ system. Overall, the charge–discharge measurements show that CS-BF_4-80 is suitable and advantageous as an excellent electrolyte in EDLC applications.

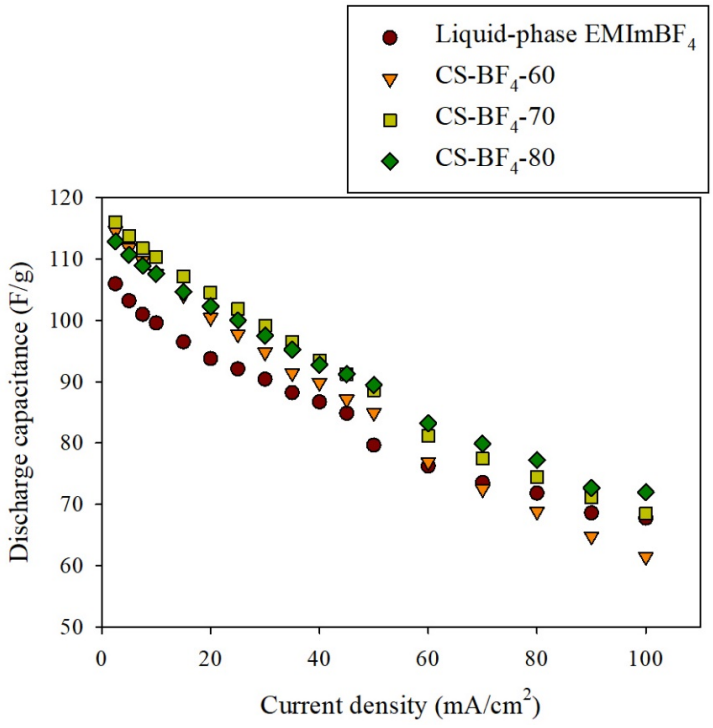

Fig. 6 Discharge capacitances of the EDLC test cell assembled with liquid-phase $EMImBF_4$ or the obtained CS-TFEs.

To investigate the electrochemical behavior at the electrode/electrolyte interface in detail, AC impedance measurements were carried out on the EDLC test cells with various types of electrolyte. Nyquist plots obtained by AC impedance measurements on the EDLC test cells assembled with liquid-phase $EMImBF_4$ or the obtained CS-TFEs are shown in Fig. 7. All test cells showed a small semicircle at high frequencies (see inset of Fig. 7), followed by a transition to linearity at low frequencies, corresponding to a capacitive behavior [64]. Focusing on the semicircles, which represent the impedance of the parallel resistance and capacitance at the contact interface between activated carbon and electrolyte [65], the observed semicircles of the CS-BF_4-60 and CS-BF_4-70 test cells are larger than that of the test cell with liquid-phase $EMImBF_4$, whereas that of the test cell with the CS-BF_4-80 test cell is slightly smaller. This shows that the higher $EMImBF_4$ content in the TFEs improved the affinity between the activated carbon and TFE, thereby reducing the electronic-contact resistance in the activated-carbon electrode at the electrode/electrolyte interface. This may be attributed to the relatively high ionicity of ILs and the highly polarizable substituents of CS such as the R–NH_2 and R–OH groups [31].

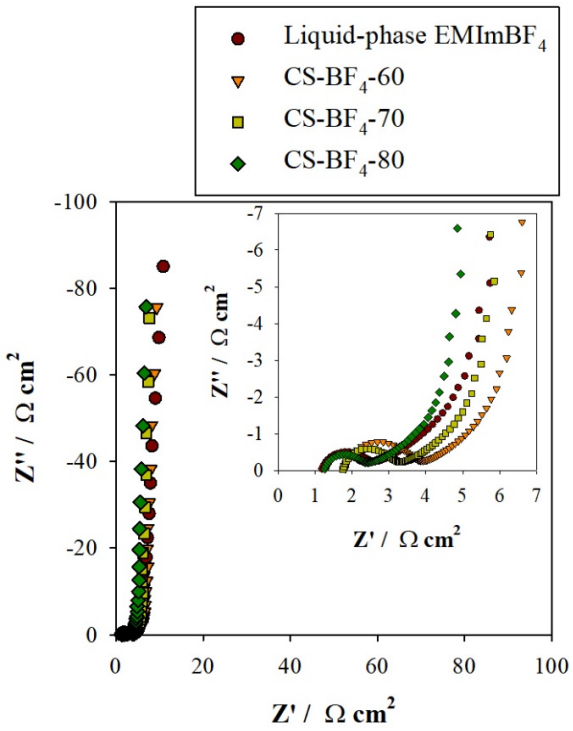

Fig. 7 Nyquist plots obtained by AC impedance measurements of the EDLC test cell assembled with the liquid-phase $EMImBF_4$ or the obtained CS-TFEs.

3.4. Conclusions

In this present work, a novel TFE as functionalized solid electrolyte was prepared from CS with $EMImBF_4$ via a new preparation method. CS powder was dissolved in a mixture of $EMImBF_4$ and DI water to produce CS-TFEs with different wt% of $EMImBF_4$ in the dry sample for the first time. In this system, $EMImBF_4$ plays important roles as a solvent and a charge carrier for EDLC applications. From structural characterizations, all of the obtained CS-TFEs from the new preparation method showed surfaces with no CS/$EMImBF_4$ phase separation, and the surface morphologies of the samples changed according to the dry-film wt% of $EMImBF_4$. The FT-IR spectra of the CS-TFE products showed peaks that were characteristic of both CS and $EMImBF_4$, indicating that $EMImBF_4$ was incorporated efficiently into the CS matrix. The TGA and DTGA results revealed that the all of the CS-TFE products had high thermal stability. The results of tensile testing showed that the obtained samples from the new preparation method had significant higher tensile strength than that of the CS-gel from previous reports. Furthermore, the

total $EMImBF_4$ content of the obtained samples (CS-BF_4-60, CS-BF_4-70, and CS-BF_4-80) is 51.1%, 58.0%, and 78.8%, respectively, and could be controlled by the preparation conditions of the CS solutions.

In addition, the obtained CS-TFEs were fabricated in EDLC test cells to measure their electrochemical properties in comparison with that of a test cell with a liquid-phase $EMImBF_4$ system. On testing the charge–discharge performance, the CS-BF_4-80 test cell exhibited an *IR* drop at high current density that was comparable to that of the liquid-phase $EMImBF_4$ test cell, and the former also showed a higher discharge capacitance over the current-density range of 2.5–100 mA/cm^2. Moreover, the results of the AC impedance measurements on the CS-BF_4-80 test cell showed decreased resistance at the electrode/electrolyte interface compared with the liquid-phase $EMImBF_4$ test cell. All of the results regarding electrochemical properties showed the CS-BF_4-80 TFE to be suitable and advantageous as an excellent solid electrolyte in the design of high-performance EDLCs, as well as for improving the safety of such devices.

3.5. References

[1] S. Kumagai, D. Tashima, Biomass Bioenergy 83, 216–223 (2015)

[2] A. Mundy, G.L. Plett, J. Energy Storage 7, 167–180 (2016)

[3] M. Tokita, N. Yoshimoto, K. Fujii, M. Morita, Electrochim. Acta 209, 210–218 (2016)

[4] M. Yamagata, K. Soeda, S. Yamazaki, M. Ishikawa, J. Electrochem. Soc. 25(35), 193–200 (2010)

[5] M. Yamagata, S. Ikebe, Y. Kasai, K. Soeda, M. Ishikawa, J. Electrochem. Soc. 50(43), 27–36 (2013)

[6] K. Soeda, M. Yamagata, M. Ishikawa, J. Power Sources 280, 565–572 (2015)

[7] N.N. Mobarak, N. Ramli, A. Ahmad, M.Y.A. Rahman, Solid State Ionics 224, 51–57 (2012)

[8] S. Rudhziah, M.S.A. Rani, A. Ahmad, N.S. Mohamed, H. Kaddami, Ind. Crops Prod. 72, 133–141 (2015)

[9] E. Raphael, C.O. Avellaneda, B. Manzolli, A. Pawlicka, Electrochim. Acta 55, 1455–1459 (2010)

[10] R. Leones, F. Sentanin, L.C. Rodrigues, I.M. Marrucho, J.M.S.S. Esperança, A. Pawlicka,

M.M. Silva, eXPRESS polym. lett. 6(12), 1007–1016 (2012)
[11] A.S.A. Khiar, A.K. Arof, Ionics 16, 123–129 (2010)
[12] M. Kumar, T. Tiwari, N. Srivastava, Carbohydr. Polym. 88, 54–60 (2012)
[13] M.F. Shukur, R. Ithnin, M.F.Z. Kadir, Electrochim. Acta 136, 204–216 (2014)
[14] A.M.M. Ali, R.H.Y. Subban, H. Bahron, T. Winie, F. Latif, M.Z.A. Yahya, Ionics 14 491–500 (2008)
[15] S.N. Mohamed, N.A. Johari, A.M.M. Ali, M.K. Harun, M.Z.A. Yahya, J. Power Sources 183, 351–354 (2008)
[16] R.K. Mishra, A. Anis, S. Mondal, M. Dutt, A.K. Banthia, Chin. J. Polym. Sci. 27(5), 639–646 (2009)
[17] R. Ou, Y. Xie, X. Shen, F. Yuan, H. Wang, Q. Wang, J. Mater. Sci. 47, 5978–5986 (2012)
[18] R. Alves, F. Sentanin, R.C. Sabadini, A. Pawlicka, M.M. Silva, Electrochim. Acta 217 108–116 (2016)
[19] R. Leones, P.M. Reis, R.C. Sabadini, L.P. Ravaro, I.D.A. Silva, A.S.S. de Camargo, J.P. Donoso, C.J. Magon, J.M.S.S. Esperança, A. Pawlicka, M.M. Silva, Electrochim. Acta 240 474–485 (2017)
[20] R. Leones, R.C. Sabadini, J.M.S.S. Esperança, A. Pawlicka, Electrochim. Acta 232 22–29 (2017)
[21] R. Jayakumar, H. Nagahama, T. Furuike, H. Tamura, Int. J. Biol. Macromol. 42, 335–339 (2008)
[22] A. Anitha, V.V.D. Rani, R. Krishna, V. Sreeja, N. Selvamurugan, S.V. Nair, H. Tamura, R. Jayakumar, Carbohydr. Polym. 78, 672–677 (2009)
[23] K. Madhumathi, K.T. Shalumon, V.V.D. Rani, H. Tamura, T. Furuike, N. Selvamurugan, S.V. Nair, R. Jayakumar, Int. J. Biol. Macromol. 45, 12–15 (2009)
[24] H. Nagahama, H. Maeda, T. Kashiki, R. Jayakumar, T. Furuike, H. Tamura, Carbohydr. Polym. 76, 255–260 (2009)
[25] Y. Saito, V. Luchnikov, A. Inaba, K. Tamura, Carbohydr. Polym. 109, 44–48 (2014)
[26] T. Furuike, D. Komoto, H. Hashimoto, H. Tamura, Int. J. Biol. Macromol. 104, 1620–1625 (2017)
[27] R. Jayakumar, N. Selvamurugan, S.V. Nair, S. Tokura, H. Tamura, Int. J. Biol. Macromol. 43, 221–225 (2008)

[28] R. Jayakumar, M. Prabaharan, S.V. Nair, H. Tamura, Biotechnol. Adv. 28, 142–150 (2010)

[29] R. Jayakumar, M. Prabaharan, P.T. Sudheesh Kumar, S.V. Nair, H. Tamura, Biotechnol. Adv. 29, 322–337 (2011).

[30] M. Yamagata, K. Soeda, S. Ikebe, S. Yamazaki, M. Ishikawa, J. Electrochem. Soc. 41, 25–34 (2012)

[31] M. Yamagata, K. Soeda, S. Ikebe, S. Yamazaki, M. Ishikawa, Electrochim. Acta 100, 275–280 (2013)

[32] K. Soeda, M. Yamagata, S. Yamazaki, M. Ishikawa, Electrochemistry 81(10), 867–872 (2013)

[33] J. Chupp, A. Shellikeri, G. Palui, J. Chatterjee, J. Appl. Polym. Sci. 132(26), 42143 (2015)

[34] X. Mu, X. Yang, D. Zhang, C. Liu, Carbohydr. Polym. 146, 46–51 (2016)

[35] W. Wang, J. Zhu, X. Wang, Y. Huang, Y. Wang, J. Macromol. Sci., Part B 49 (3), 528–541 (2010)

[36] K. Wilpiszewska, T. Spychaj, Carbohydr. Polym. 86, 424–428 (2011)

[37] A. Lewandowski, M. Galiński, J. Phys. Chem. Solids 65, 281–286 (2004)

[38] Z. Zhou, M. Takeda, M. Ue, J. Fluorine Chem. 125, 471–476 (2004)

[39] T. Sato, G. Masuda, K. Takagi, Electrochim. Acta 49, 3603–3611 (2004)

[40] K. Yuyama, G. Masuda, H. Yoshida, T. Sato, J. Power Sources 162, 1401–1408 (2006)

[41] C.O. Ania, J. Pernak, F. Stefaniak, E. Raymundo-Piñero, F. Béguin, Carbon 44, 3126–3130 (2006)

[42] N. Handa, T. Sugimoto, M. Yamagata, M. Kikuta, M. Kono, M. Ishikawa, J. Power Sources 185, 1585–1588 (2008)

[43] D.M. Phillips, L.F. Drummy, D.G. Conrady, D.M. Fox, R.R. Naik, M.O. Stone, P.C. Trulove, H.C. De Long, R.A. Mantz, J. Am. Chem. Soc. 126, 14350–14351 (2004)

[44] O.A.E. Seoud, A. Koschella, L.C. Fidale, S. Dorn, T. Heinze, Biomacromolecules 8(9), 2629–2647 (2007)

[45] I. Kilpeläinen, H. Xie, A. King, M. Granstrom, S. Heikkinen, D.S. Argyropoulos, J. Agric. Food Chem. 55, 9142–9148, (2007)

[46] R.P. Swatloski, S.K. Spear, J.D. Holbrey, R.D. Rogers, J. Am. Chem. Soc. 124, 4974–4975 (2002)

[47] M.E. Zakrzewska, E. Bogel-Łukasik, R. Bogel-Łukasik, Energy Fuels 24, 737–745 (2010)

[48] B. Meenatchi, V. Renuga, A. Manikandan, J. Mol. Liq. 238, 582–588 (2017)
[49] H. Xie, S. Zhang, S. Lib, Green Chem. 8, 630–633 (2006)
[50] W. Xiao, Q. Chen, Y. Wu, T. Wu, L. Dai, Carbohydr. Polym. 83, 233–238 (2011)
[51] S.S. Silva, J.F. Mano, R.L. Reis, Green Chem. 19, 1208–1220 (2017)
[52] G. Santos-López, W. Argüelles-Monal, E. Carvajal-Millan, Y.L. López-Franco, M.T. Recillas-Mota, J. Lizardi-Mendoza, Polym. 9, 722 (2017)
[53] Q. Chen, A. Xu, Z. Li, J. Wang, S. Zhang, Green Chem. 13, 3446–3452 (2011)
[54] X. Sun, Q. Tian, Z. Xue, Y. Zhang, T. Mu, RSC Adv. 4, 30282–30291 (2014)
[55] Q. Tian, S. Liu, X. Sun, H. Sun, Z. Xue, T. Mu, Carbohydr. Res. 408, 107–113 (2015)
[56] S. Kumari, S.H.K. Annamareddy, S. Abanti, P.K. Rath, Int. J. Biol. Macromol. 104, 1697–1705 (2017)
[57] R.A. Mauricio-Sánchez, R. Salazar, J.G. Luna-Bárcenas, A. Mendoza-Galván, Vib. Spectrosc 94, 1–6 (2018)
[58] Y. Wang, X. Gao, R. Wang, H. Liu, C. Yang, Y. Xiong, React. Funct. Polym. 68, 1170–1177 (2008)
[59] S. Ambika, M. Sundrarajan, J. Mol. Liq. 221, 986–992 (2016)
[60] T. Romann, O. Oll, P. Pikma, H. Tamme, E. Lust, Electrochim. Acta 125, 183–190 (2014)
[61] C.Y. Soon, Y.B. Tee, C.H. Tan, A.T. Rosnita, A. Khalina, Int. J. Biol. Macromol. 108, 135–142 (2018)
[62] G. Min, T. Yim, H.Y. Lee, D.H. Huh, E. Lee, J. Mun, S.M. Oh, Y.G. Kim, Bull. Korean Chem. Soc. 27(6), 847–852 (2006)
[63] Y. Cao, T. Mu, Ind. Eng. Chem. Res. 53, 8651–8664 (2014)
[64] C. Yang, S. Hsu, W. Chien, J. Power Sources 152, 303–310 (2005)
[65] A. Lewandowski, A. Świderska, Solid State Ionics 161, 243–249 (2003)

Chapter 4

Preparation and Characterization of Electrospun Gelatin Nanofiber Electrolyte

4.1. Introduction

Electric double-layer capacitors (EDLCs) are electrochemical devices that provide a high sustained power density and a long charge–discharge cycle time [1, 2]. Nonaqueous electrolytes have been proposed in recent years to satisfy the safety requirements for EDLCs [3–7]. Polymer electrolytes based on natural polymers such as chitosan [8–10], alginate [11–13], agar [14, 15], carrageen [16–19], starch [20–22] and bacterial cellulose [23] have been widely studied. In addition to being abundant, low cost, non-toxic, and environmentally friendly, natural polymers have been reported to have good physical and mechanical properties and high thermal stabilities. Gelatin is prepared by the hydrolysis of collagen, which is a natural, triple-helix polymer obtained from mammalian skin and bones [24, 25]. Gelatin has been widely used as a scaffold for tissue engineering owing to its excellent biodegradability, biocompatibility, ability to promote cell adhesion and proliferation, resistance to immunogenicity, among other properties [26–30]. Moreover, many researches have reported that gelatin has potential to be used as an electrolyte in many applications such as in dye-sensitized solar cells and electrochromic devices [31–36].

Gelatin is soluble in lukewarm water and forms a heterogeneous mixture. An important property of gelatin is its gelation transition under aqueous conditions [37]. Gelatin is also compatible with electrospinning, which is a simple and cost-effective technique that is widely used to simply and continuously fabricate nanofibers. Electrospun fibers offer small pores, high surface area, physical stability, and controllable thickness in the membrane form. Thus, electrospinning is an attractive option for fabricating gel electrolytes to apply in EDLCs.

In this chapter, we fabricate a novel gel electrolyte from gelatin via an electrospinning technique. We focus on one potential application of the electrolyte in EDLCs for improved device safety. The novel gel electrolyte was characterized, and the electrochemical properties of EDLC test cells assembled with the following electrolytes were compared: gelatin electrospun (GES) electrolytes soaked in 1-ethyl-3-methylimidazolium ($EMImBF_4$), gelatin films containing $EMImBF_4$ (GF-BF_4), which were further soaked in $EMImBF_4$, and pure $EMImBF_4$ including a separator.

4.2. Materials and methods

4.2.1. Materials

Gelatin (JS200, Mw = 100,000, bovine skin type B, Lot No. 120705M), was purchased in powder form from Koei Chemical Co., Ltd (Japan) and 1-ethyl-3-methylimidazolium tetrafluoroborate ($EMImBF_4$, 99.0%) was purchased from Toyo Gosei Co., Ltd (Japan).

4.2.2. Preparation of GES electrolytes

Gelatin powder was dissolved at 25 wt% in deionized (DI) water and the mixture was stirred at 50°C until a homogeneous solution was obtained. The solution was left in a water bath at 50°C for about 1 h to remove entrapped air and was then cooled in an ice bath to induce gelation. The gelated gelatin was placed in a 5-mL syringe with a metal needle of diameter 1.5 mm, and the syringe was placed in a water bath at 50°C to reverse the gelation; the temperature of the syringe was thereafter maintained at 45°C–50°C. A high-voltage power supply of 23 kV was connected to the syringe needle tip and to a stationary collector covered with aluminum foil. The tip-to-collector distance was set at 7 cm. The electrospun nanofibers were collected as randomly overlaid mats on the electrically grounded plate. The spinning time was varied to 5, 10, 15 20, and 25 min. The gelatin electrospun samples were then dried at room temperature for 12 h before being removed from the aluminum foil for use in further testing.

4.2.3. Preparation of GF-BF_4

For comparison with the GES electrolytes, GF-BF_4 electrolytes were prepared as follows. In a glass bottle, gelatin powder was mixed at 30 wt% in DI water with $EMImBF_4$ at different concentrations, as listed in Table 1, in a glass bottle. The mixture was stirred at 50°C until it became a homogeneous solution. Then, the solution was casted on a Teflon sheet with a 135-μm leveled supporter. The GF-BF_4 electrolytes were dried at 60°C before use in further testing.

Table 1 Composition of gelatin solutions for GF-BF_4 electrolytes.

Sample	Weight of gelatin (g)	Weight of DI water (g)	Weight of $EMImBF_4$ (g)	wt% of $EMImBF_4$ in dry film
GF-BF_4-45	1.5	2.3	1.2	45
GF-BF_4-50	1.5	2.0	1.5	50
GF-BF_4-55	1.5	1.7	1.8	55

4.2.4. Characterization of GES electrolytes

4.2.4.1. Fourier transform infrared spectroscopy (FTIR)

To identify the function groups present in the obtained samples, they were ground and mixed thoroughly with potassium bromide and were analyzed using Fourier transfer infrared spectroscopy (FTIR; 670-IR, VARIAN Inc., USA).

4.2.4.2. Thermogravimetric analysis (TGA)

A thermo-gravimetric/differential thermal analyzer (TGA/DTG; EXSTAR TG/DTA6200, SII, Japan) was used to measure the thermal properties of the obtained samples. All samples were vacuum dried at room temperature for one day before analysis. The samples were tested at a heating rate of 20°C/min in the range 30°C–500°C under a nitrogen atmosphere.

4.2.4.3. Scanning electron microscopy (SEM)

The morphologies of the obtained samples were analyzed via scanning electron microscopy (SEM; JSM6700, JEOL, Japan) at an accelerating voltage of 5 kV with 500x magnification.

4.2.4.4. Membrane thickness and mechanical properties

The thicknesses of the obtained samples were measured by a digital micrometer (IP65, Mitutoyo, Japan). The mechanical properties of the obtained samples were analyzed using a universal testing machine (STA-1150, A&D Company, Ltd, Japan) equipped with a 50-N load cell and elongated at a constant speed of 10 mm/min under ambient conditions. The test samples were cut to 30 mm in length and 5 mm in width and were mounted in the tensile grips spaced 10 mm apart before analysis.

4.2.4.5. Determination of resistance to $EMImBF_4$ damage

The resistance of GES samples to $EMImBF_4$ damage was measured after immersion in $EMImBF_4$ at room temperature, incubation in a desiccator for 10 days, and washing with ethanol. The structural morphology of the GES samples was observed using SEM before and after immersion in $EMImBF_4$.

4.2.5. Fabrication of EDLCs cells

Composite carbon electrodes were prepared by mixing activated carbon (YP-50F, Kuraray Co., Ltd, Japan), acetylene black (HS-100, Denka company Ltd, Japan) as a conductive additive, 1.2 wt% sodium carboxymethyl cellulose (WS-C, DKS Co., Ltd, Japan) as a dispersant and 48% wt styrene-butadiene rubber (TRD2001, JSR corporation, Japan) as a binder in DI water at a ratio of 90:5:3:2 (w/w). The slurry was then cast onto an etched aluminium-foil current collector and dried, and the obtained composite electrode sheet was cut into 12 mm-diameter disks. Two carbon electrodes were immersed in $EMImBF_4$ for 10 min under reduced pressure while the gel electrolyte was soaked in $EMImBF_4$ under a 0.3 Pa vacuum at room temperature for 48 h. The test cells were then assembled with the prepared carbon electrodes and gel electrolytes. In addition, test cells were assembled with liquid-phase $EMImBF_4$ and a cellulose separator (TF4035, Nippon Kodoshi Corporation, Japan) for comparison. The whole assembly procedure was performed in an argon-filled glove box.

4.2.6. Electrochemical measurement

The electrochemical properties of EDLC test cells were measured in terms of the charge–discharge characteristics, discharge capacitance and AC impedance of each test cell. The performance was measured using a battery charge/discharge apparatus (HJ1001 SM8, Hokuto Denko Corporation, Japan). The charge–discharge tests were carried out in the voltage range between 0 and 2.5 V at various densities. The discharge rate was estimated at various discharge current densities between 2.5 and 100 mA/cm^2 when a constant current was charged up to 2.5 V. The discharge capacitance of a single electrode in the EDLC symmetrical cells was determined using Eq. (1) [8–12]:

$$C = \left(\frac{I \times t}{(V/2) \times W} \right) \tag{1}$$

where C is the discharge capacitance, I is the discharge current (A), t is the discharge time (s), V is the operating voltage, W is the total mass of activated carbon in a single electrode (g).

AC impedance measurements were taken using a potentiogalvanostat (SI 1287 type, Solartron Analytical, UK) and a frequency-response analyzer (SI 1260 type, Solartron Analytical, UK) with an AC amplitude of 10 $mV_{p\text{-}0}$ in the frequency range of 500 kHz–10 mHz. All electrochemical measurements were performed at 25°C.

4.3. Results and discussion

4.3.1. Characterization of GES electrolytes

4.3.1.1. FTIR

The FTIR spectra of gelatin powder and GES fibers fabricated with spinning times of 5, 10, 15, 20, and 25 min (labeled as GES-5, GES-10, GES-15, GES-20, and GES-25, respective) are shown in Fig. 1. All samples showed similar absorption peaks. The characteristic peaks were interpreted as follows: stretching of N–H and hydrogen bonding are

observed around 3300 cm^{-1} (amide A), stretching of C=O is observed around 1650 cm^{-1} (amide I), bending and stretching of N–H is observed at 1540 cm^{-1} (amide II) and stretching of C–N and bending of N–H are observed at 1240 cm^{-1}. These absorption peaks are characteristic of gelatin [26], [38] so the presence of these peaks proves that the electrospinning process did not alter the functional groups of the gelatin.

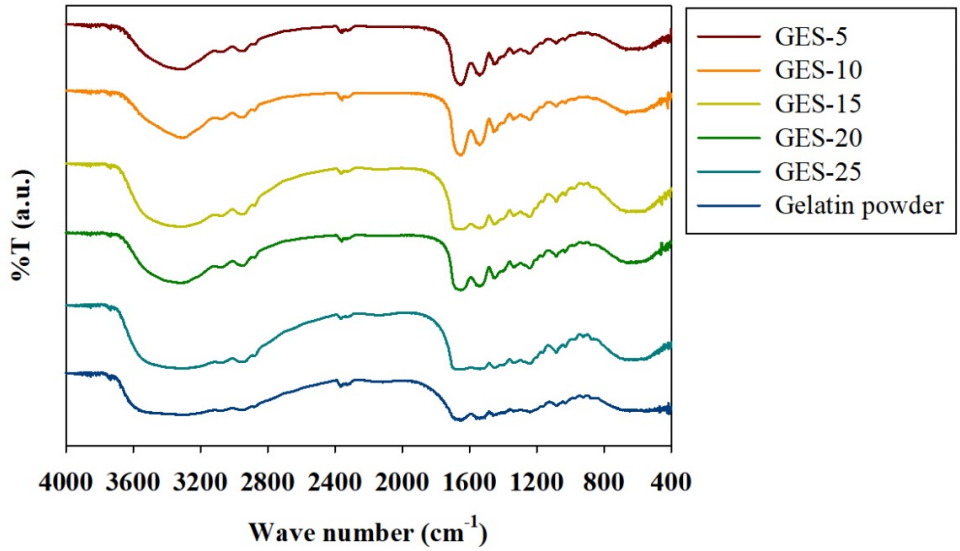

Fig. 1 FTIR spectra of gelatin powder and GES products.

4.3.1.2. TGA

TGA and DTG thermograms of gelatin powder and the GES products are shown in Fig. 2. All samples demonstrated an initial weight loss due to evaporation of the moisture on the surface in the temperature range of 40–130°C. The moisture content of the GES products was higher than that of the gelatin powder because of the comparatively high surface area of the GES fibers. The onset of the second weight loss occurred around 200°C and the maximum weight loss occurred at approximately 330°C due to the degradation of the protein [39, 40]. These results demonstrate high thermal stability and imply that GES fibers may potentially be used as gel electrolytes in EDLCs under high-temperature operation.

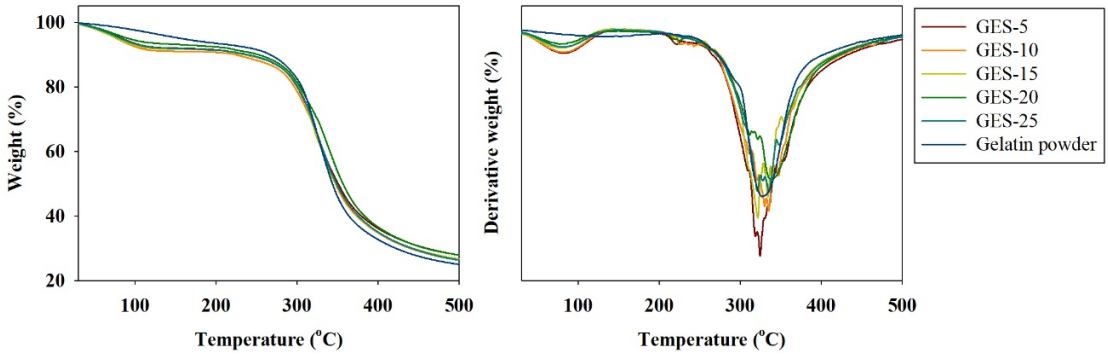

(a) (b)

Fig. 2 (a) TGA and (b) DTG thermograms of gelatin powder and GES products.

4.3.1.3. SEM

SEM images of the GES products as well as the fiber-diameter distribution measured from the SEM images are shown in Fig. 3. The SEM images revealed a clearly nanofibrous structure with an average fiber diameter of approximately 306.2–428.4 nm. Moreover, SEM images of GF-BF_4 electrolytes with varying ratios of $EMImBF_4$ are shown in Fig. 4. The surfaces of all GF-BF_4 samples displayed disuniformity and a phase separation between the gelatin and $EMImBF_4$. This may have arisen from excess $EMImBF_4$ that was not incorporated into the matrix.

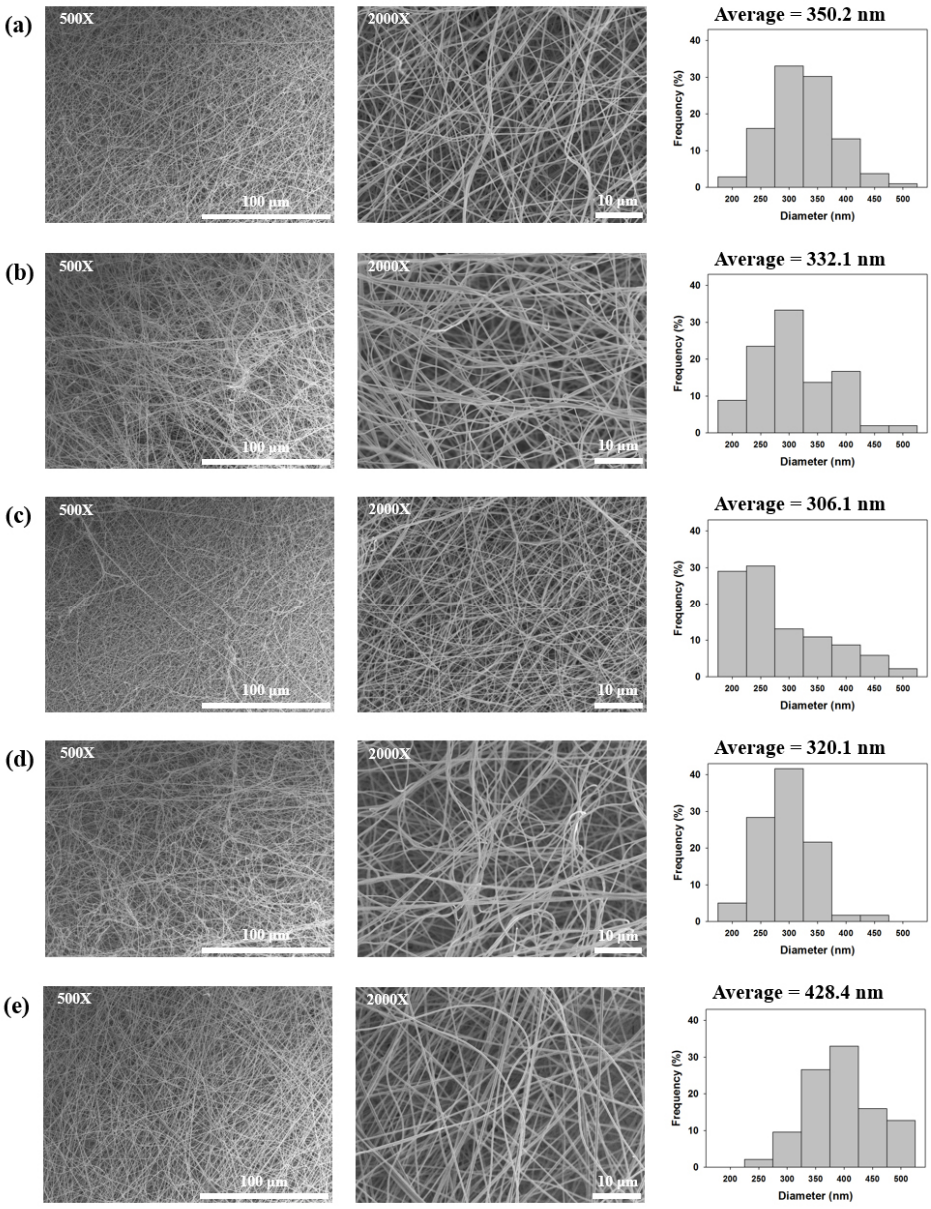

Fig. 3 SEM images with 500 and 2000 magnification and the measured fiber-diameter distribution of (a) GES-5, (b) GES-10, (c) GES-15, (d) GES-20 and (e) GES-25.

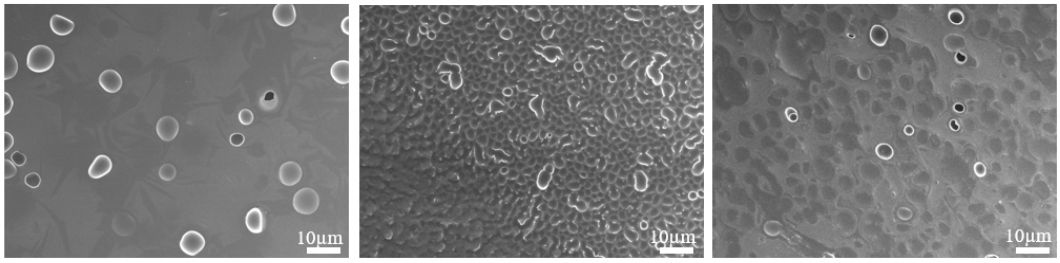

(a) (b) (c)

Fig. 4 SEM images of (a) GF-BF_4-45, (b) GF-BF_4-50 and (c) GF-BF_4-55.

4.3.1.4. Membrane thickness and mechanical properties

The thickness, tensile strength, and % elongation at break of the GES products are shown in Table 2. The thicknesses of the membranes were greater with higher spinning times. This result is consistent with the tensile-strength results: the tensile strength was greater in membranes fabricated with higher spinning times. On the contrary, the elongation at break of the GES products showed no tendency to increase or decrease with the spinning time, exhibiting an average of 13% elongation at break. This may have been due to the fibrous structure of the samples. Based on these results, the GES-25 sample showed the highest tensile strength with a thickness, which is suitable for use as a gel electrolyte in EDLCs. Thus, GES-25 was chosen for the following electrochemical tests.

Table 2 Thickness and mechanical properties of GES products.

Sample	Thickness (μm)	Tensile strength (cN)	Elongation at break (%)
GES-5	25.5 ± 3.8	29.6 ± 11.6	11.6 ± 3.0
GES-10	34.8 ± 5.6	50.2 ± 22.5	11.3 ± 4.5
GES-15	46.1 ± 6.2	78.2 ± 35.0	14.5 ± 4.2
GES-20	72.4 ± 9.3	90.4 ± 24.5	13.3 ± 4.1
GES-25	76.4 ± 8.8	147.3 ± 33.7	15.8 ± 3.0

4.3.1.5. Determination of resistance to $EMImBF_4$ damage

The GES-25 before and after 10 days of immersion in $EMImBF_4$ are shown in Fig. 5. The results showed that the nanofibers of GES-25 were stable and were not damaged or deformed after immersion in $EMImBF_4$ at room temperature for 10 days. It should be noted that the GES nanofibers may potentially act as a host to $EMImBF_4$.

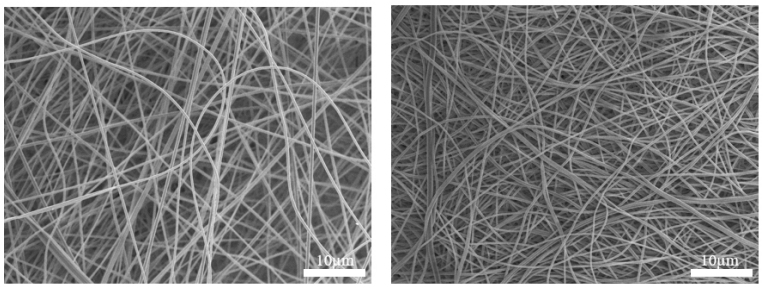

(a) (b)

Fig. 5 SEM images showing the resistance of GES-25 to $EMImBF_4$ damage; GES-25 (a) before immersion in $EMImBF_4$ and (b) after immersion in $EMImBF_4$ for 10 days.

4.3.2. Electrochemical results

The electrochemical properties of the EDLC test cell with the GES-25 gel electrolyte were measured and compared with those with GF-BF_4 electrolytes (including GF-BF_4-45, GF-BF_4-50, and GF-BF_4-55) and that with liquid-phase $EMImBF_4$ as the electrolyte. The gel electrolytes were soaked in $EMImBF_4$ before assembling the test cells.

The charge–discharge curves of EDLC test cells assembled with liquid-phase $EMImBF_4$ and with the GES-25 gel electrolyte including $EMImBF_4$ (GES-25/$EMImBF_4$) were measured at high current densities of 50 and 100 mA/cm^2 and are shown in Fig. 6(a) and 6(b), respectively. Under these high current densities, the test cell with the GES-25/$EMImBF_4$ gel electrolyte showed an IR drop at the switching point from charge to discharge which was slightly larger amount of IR drop that of the test cell with liquid-phase $EMImBF_4$ due to the ionic conductivity of test cell with the GES-25/$EMImBF_4$ lower than that liquid-phase $EMImBF_4$ system. However, the ionic conductivity of test cell with the GES-25/$EMImBF_4$ was showed

significantly higher than that of conventional gel-electrolytes composed of synthesized polymer matrix from previous reports [41]. The test cells with GF-BF_4 which were immersed in $EMImBF_4$ before assembly (GF-BF_4/$EMImBF_4$), including GF-BF_4-45/$EMImBF_4$, GF-BF_4-50/$EMImBF_4$, and GF-BF_4-55/$EMImBF_4$, could not be tested at high current densities owing of the high internal resistance of these electrolytes.

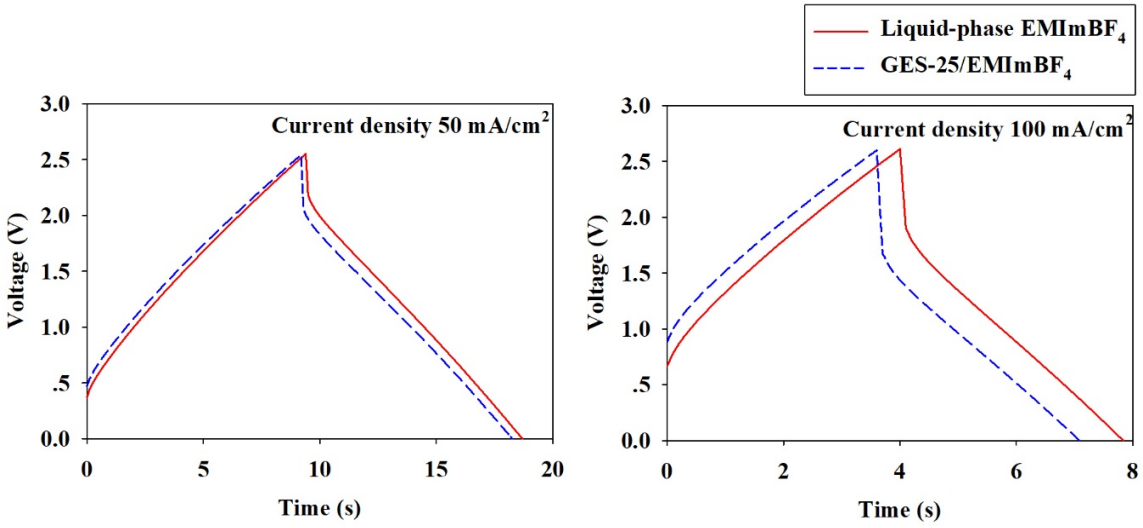

(a) (b)

Fig. 6 Charge–discharge curves of the EDLC test cells with liquid-phase $EMImBF_4$ and with GES-25/$EMImBF_4$ as the electrolytes at current densities of (a) 50 and (b) 100 mA/cm^2.

In addition, the discharge capacitances of the same EDLC test cells as a function of the applied current density in the range of 2.5–100 mA/cm^2 are shown in Fig. 7. The results demonstrate that the discharge capacitance retention of the test cell with the GES-25/$EMImBF_4$ gel electrolyte differed only slightly with that of the test cell with the liquid-phase $EMImBF_4$ electrolyte within the entire current-density range. Overall, the charge–discharge measurements indicate that GES-25/$EMImBF_4$ may be more effective as an electrolyte than liquid-phase $EMImBF_4$ in nonaqueous EDLCs for improving the safety of the devices without reducing the performance.

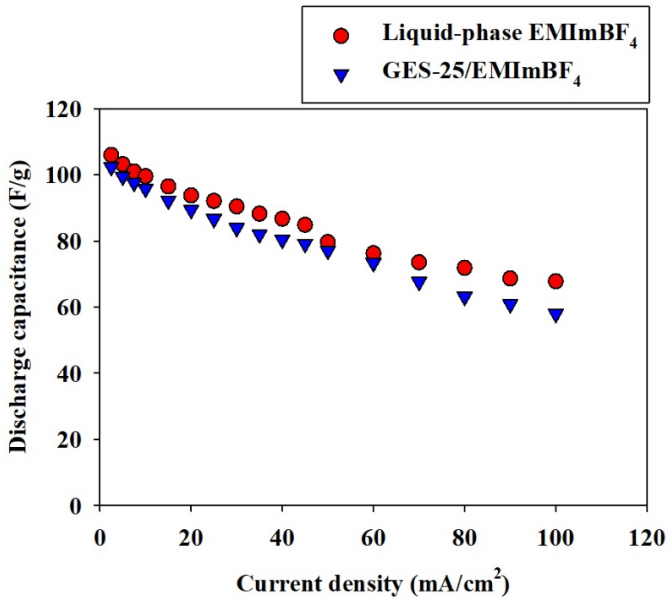

Fig. 7 Discharge capacitances of the EDLC test cells with liquid-phase $EMImBF_4$ and with GES-25/$EMImBF_4$ as the electrolytes.

The Nyquist plots of the test cells having liquid-phase $EMImBF_4$ and GES-25/$EMImBF_4$ as electrolytes and those with GF-BF_4 (including GF-BF_4-45/$EMImBF_4$, GF-BF_4-50/$EMImBF_4$, and GF-BF_4-55/$EMImBF_4$) as electrolytes are shown in Fig. 8(a) and 8(b), respectively. The resistance of the EDLC test cell with the GES-25/$EMImBF_4$ gel electrolyte was slightly higher than that of the test cell with liquid-phase $EMImBF_4$, but this difference was insignificant. For the test cell with the GES-25/$EMImBF_4$ gel electrolyte, the semicircle, which represents the impedance of parallel resistance and capacitance at a contact interface [42], such as that of the activated carbon electrode and the electrolyte of the test cell, was larger than the test cell with the liquid-phase $EMImBF_4$ electrolyte. This result indicates that the obtained GES gel electrolyte was in poor contact with the activated carbon electrode. Thus, to improve the contact surface between the GES gel electrolyte and the electrode of activated carbon is an interesting topic for future research. However, compared with the EDLC test cells with the GF-BF_4/$EMImBF_4$ electrolytes, the test cell with the GES-25/$EMImBF_4$ electrolyte showed significantly lower resistance. It should be noted that the electrospinning process with gelatin significantly improved the affinity between the activated carbon and the gel electrolyte, leading to a reduction of the electrode/gel electrolyte interface resistance at the electrode/electrolyte

interface compared with the GF-BF_4/EMImBF_4. The knowledge gained from this experiment has a potential to inform future approaches to develop gel electrolytes from gelatin for use in EDLCs.

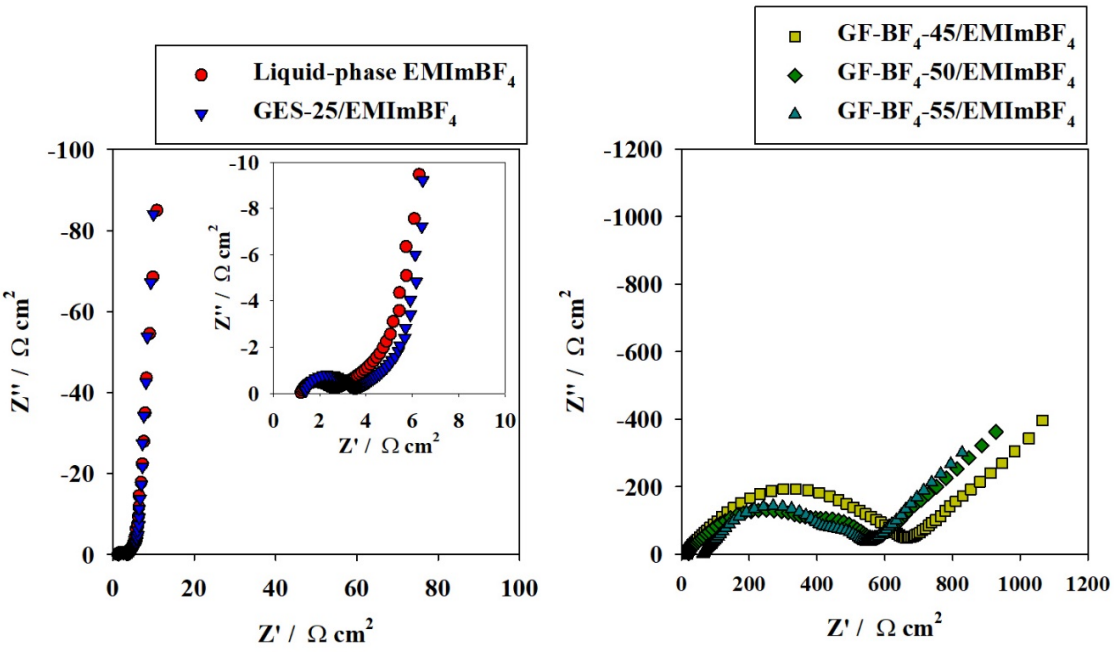

(a) (b)

Fig. 8 Nyquist plots obtained by AC impedance measurements of EDLC test cells with (a) liquid-phase EMImBF_4 and with GES-25/EMImBF_4 as the electrolytes and those with (b) GF-BF_4-45/EMImBF_4, GF-BF_4-50/EMImBF_4 and GF-BF_4-55/EMImBF_4 as the electrolytes.

4.4. Conclusions

In the present study, a novel nonaqueous gel electrolyte was successfully prepared by electrospinning of gelatin and characterized in the context of its application as both the electrolyte and the separator for EDLCs. To fabricate the electrolytes, gelatin powder was dissolved in DI water at 25 wt%. This solution was then electrospun with a range of spinning times. Based on a structural analysis, the fabricated GES electrolytes had a nanofibrous structure with fiber diameters in the range of approximately 306.2–428.4 nm. The FTIR spectra of the GES products revealed peaks which are characteristic of gelatin, indicating that there was no change in the functional groups due to the electrospinning process. Thermograms of the GES

products indicated that they had high thermal stabilities, which is a favourable property for gel electrolytes to be used in EDLCs for high-temperature operation. The thicknesses of the GES membranes increased with an increase of spinning time. The tensile testing results for the obtained samples showed that the nanofibrous structure was highly flexible and had a high tensile strength. Further, there was no change in the structure after immersing it in $EMImBF_4$ for 10 days. Then, the electrochemical properties of GES-25 were characterized in EDLC test cells.

EDLC test cells were assembled with GES (GES-25/$EMImBF_4$), GF-BF_4 (including GF-BF_4-45/$EMImBF_4$, GF-BF_4-50/$EMImBF_4$, and GF-BF_4-55/$EMImBF_4$) and pure $EMImBF_4$ as the electrolytes to measure their electrochemical properties. The test cell with the GES-25/$EMImBF_4$ gel electrolyte exhibited a comparable discharge capacitance to that of the test cell with liquid-$EMImBF_4$. The GES-25/$EMImBF_4$ test cell also had a superior electrode/gel electrolyte interface resistance at the electrode/electrolyte interface compared with the test cells with the GF-BF_4/$EMImBF_4$ electrolytes. The electrochemical characteristics suggested that the novel nonaqueous gel electrolyte of GES nanofibers proposed here can be employed as a useful gel electrolyte for solid-stage electrolyte in EDLCs, thereby improving the safety of such devices.

4.5. References

[1] A. Mundy, G.L. Pleet, J. Energy Storage 7, 167–180 (2016)

[2] M. Tokita, N. Yoshimoto, K. Fujii, M. Morita, Electrochim. Acta 209, 210–218 (2016)

[3] B. Rupp, M. Schmuck, A. Balducci, M. Winter, W. Kern, Eur. Polym. J. 44, 2986–2990 (2008)

[4] M. Rao, X. Geng, Y. Liao, S. Hu, W. Li, J. Membr. Sci. 399–400, 37–42 (2012)

[5] P.F.R. Ortega, J.P.C. Trigueiro, G.G. Silva, R.L. Lavall, Electrochim. Acta 188, 809–817 (2016)

[6] M. Safa, A. Chamaani, N. Chawla, B. El-Zahab, Electrochim. Acta 213, 587–593 (2016)

[7] J. Rymarczyk, M. Carewska, G. B. Appetcchi, D. Zane, F. Alessandrini, S. Passerini, Eur. Polym. J. 44, 2153–2161 (2008)

[8] K. Soeda, M. Yamagata, S. Yamazaki, M. Ishikawa, Electrochemistry 81(10), 867–872 (2013)

[9] M. Yamagata, K. Soeda, S. Ikebe, S. Yamazaki, M. Ishikawa, Electrochim. Acta 100, 275–280 (2013)

[10] M. Yamagata, K. Soeda, S. Ikebe, S. Yamazaki, M. Ishikawa, J. Electrochem. Soc. 41(22), 25–35 (2012)

[11] M. Yamagata, S. Ikebe, Y. Kasai, K. Soeda, M. Ishikawa, J. Electrochem. Soc. 50(43), 27–36 (2013)

[12] K. Soeda, M. Yamagata, M. Ishikawa, J. Power Sources 280, 565–572 (2015)

[13] M. Yamagata, K. Soeda, S. Yamazaki, M. Ishikawa, J. Electrochem. Soc. 25(35), 193–200 (2010)

[14] E. Raphael, C.O. Avellaneda, B. Manzolli, A. Pawlicka, Electrochim. Acta 55, 1455–1459 (2010)

[15] R. Leones, F. Sentanin, L.C. Rodrigues, I.M. Marrucho, J.M.S.S. Esperança, A. Pawlicka, M.M. Silval, Express Polym. Lett. 6(12), 1007–1016 (2012)

[16] S. Rudhziah, M.S.A. Rani, A. Ahmad, N.S. Mohamed, H. Kaddami, Ind Crops Prod 72, 133–141 (2015)

[17] N.N. Mobarak, N. Ramli, A. Ahmad and M.Y.A. Rahman, Solid State Ionics 224, 51–57 (2012)

[18] N.N. Mobarak, F.N. Jumaah, M.A. Ghani, M.P. Abdullah and A. Ahmad, Electrochim. Acta 175, 224–231 (2015)

[19] T.M. Di Palma, F. Migliardini, D. Caputo, P. Corbo, Carbohydr. Polym. 157, 122–127 (2017)

[20] A.S. Ahmad Khiar, A.K. Arof, Ionics 16, 123–129 (2010)

[21] M. Kumar, T. Tiwari, N. Srivastava, Carbohydr. Polym. 88, 54–60 (2012)

[22] M.F. Shukur, R. Ithnin, M.F.Z. Kadir, Electrochim. Acta 136, 204–216 (2014)

[23] D. Kotatha, K. Morishima, S. Uchidd, M. Ogino, M. Ishikawa, T. Furuike, H. Tamura, Res. Chem. Intermediat. 44(8), 4971–4987 (2018)

[24] T. Furuike, T. Chaochai, T. Okubo, T. Mori, H. Tamura, Int. J. Biol. Macromol. 93, 1530–1538 (2016)

[25] M. Peter, N. Ganesh, N. Selvamurugan, S.V. Nair, T. Furuike, H. Tamura, R. Jayakumar, Carbohydr. Polym. 80, 687–694 (2010)

[26] L. Ji, W. Qiao, Y. Zhang, H. Wu, S. Miao, Z. Cheng, Q. Gong, J. Liang, A. Zhu, Mater. Sci. Eng., C 78, 362–369 (2017)

[27] X. Liu, P.X. Ma, Biomaterials 30, 4094–4103 (2009)

[28] M.B. Dainiak, I.U. Allan, I.N. Savina, L. Cornelio, E.S. James, S.L. James, S.V. Mikhalovsky, H. Jungvid, I.Y. Galaev, Biomaterials 31, 67–76 (2010)

[29] F. Zhang, C. He, L. Cao, W. Feng, H. Wang, X. Mo, J. Wang, Int. J. Biol. Macromol. 48, 474–481 (2011)

[30] T. Billiet, E. Gevaert, T.D. Schryver, M. Cornelissen, P. Dubruel, Biomaterials 35, 49–62 (2014)

[31] R. Ramadan, H. Kamal, H.M. Hashem, K. Abdel-Hady, Sol. Energy Mater. Sol. Cells 127, 147–156 (2014)

[32] M. Khannam, R. Boruah, S.K. Dolui, J. Photochem. Photobiol., A 335, 248–258 (2017)

[33] Z. Tang, J. Wu, Q. Liu, M. Zheng, Q. Tang, Z. Lan, J. Lin, J. Power Sources 203, 282–287 (2012)

[34] R. Leones, F. Sentanin, L.C. Rodrigues, R.A.S. Ferreira, I.M. Marrucho, J.M.S.S. Esperança, A. Pawlicka, L.D. Carlos, M.M. Silva, Opt. Mater. 35, 187–195 (2012)

[35] D.F. Vieira, C.O. Avellaneda and A. Pawlicka, Electrochim. Acta 53, 1404–1408 (2007)

[36] C.O. Avellaneda, D.F. Vieira, A. Al-Kahlout, S. Heusing, E.R. Leite, A. Pawlicka, M.A. Aegerter, Sol. Energy Mater. Sol. Cells 92, 228–233 (2008)

[37] H. Nagahama, H. Maeda, T. Kashiki, R. Jayakumar, T. Furuike, H. Tamura, Carbohydr. Polym. 76, 255–260 (2009)

[38] T. Chaochai, Y. Imai, T. Furuike, H. Tamura, Fibers 4(2), 1–11 (2016)

[39] K. Jalaja, V.S. Sreehari, P.R.A. Kumar, R.J. Nirmala, Mater. Sci. Eng., C 64, 11–19 (2016)

[40] D.M. Correia, J. Padrão, L.R. Rodrigues, F. Dourado, S. Lanceros-Méndez, V. Sencadas Polym. Test. 32, 995–1000 (2013)

[41] X. Liu, T. Osaka, J. Electrochem. Soc. 144, 3066–3071 (1997)

[42] A. Lewandowski, A. Świderska, Solid State Ionics 161, 243–249 (2003)

Chapter 5

Concluding Remarks

This thesis summarizes the results of preparation and characterization of novel nonaqueous electrolyte from various natural polymers for use in electric double-layer capacitors (EDLC). In addition, EDLCs test cell have been fabricated using these new electrolytes for electrochemical properties measurements; the charge–discharge performance, the discharge capacitance, and alternating-current impedance, compare to testing cells using pure $EMImBF_4$ with a separator as the electrolyte.

In chapter 1, general introduction and background describing about EDLC and IL including the brief detail of natural polymers which was used for preparing nonaqueous electrolyte in this research; bacterial cellulose, chitosan, alginate and gelatin.

In chapter 2, A novel gel electrolyte has been prepared using bacterial cellulose (BC) coated with chitosan (CTS) and alginate (Alg) layers, which contain 1-ethyl-3-methylimidazolium tetrafluoroborate ($EMImBF_4$). The inoculated BC was oxidized and coated with alternating layers of CTS and Alg via ionic crosslinking to produce the gel electrolytes. The CTS content of the obtained gel electrolytes linearly increased with an increase in the number of CTS and Alg layers on the BC fibers. The results imply that the CTS and Alg layers successfully bound onto each fiber of BC, which was consistent with FTIR measurements. Based on a structural analysis, the fabricated gel electrolytes had a nanofibrous structure with a fiber diameter range of approximately 78.6–99.0 nm, a high thermal stability, and a significantly improved tensile strength compared to gel electrolytes of only CTS or Alg. In addition, the EDLCs test cell with a gel electrolyte of BC coated with 15 layers of CTS and Alg containing $EMImBF_4$ showed a high discharge capacitance, implying that the high affinity of this gel electrolyte for the activated-carbon electrode leads to reduced electrode/electrolyte interfacial resistance, which shows the potential of this approach compared with liquid-phase $EMImBF_4$ to obtain high-performance, safety-oriented EDLCs.

In chapter 3, A novel thin-film electrolyte (TFE) based on chitosan (CS) with $EMImBF_4$ was prepared by a new procedure. In this system, $EMImBF_4$ plays important roles as both a dissolving solution and a charge carrier for EDLC application. Through analysis and characterization of the obtained products, the CS-TEFs showed a surface without separation of phase between CS and $EMImBF_4$. The FT-IR spectra revealed peaks which are characteristic of CS including $EMImBF_4$ that confirm an effective introduction of $EMImBF_4$ into the CS matrix. The thermograms and tensile testing results indicated that these CS-TEFs had high thermal

stabilities with good tensile strength, which is a favorable property for solid-electrolyte to be used in EDLCs. Moreover, the EDLCs test cell with CS-TFE with a calculated dry thin-film content of 80 wt% $EMImBF_4$ showed a comparable IR drop and higher discharge capacitance than a liquid-phase $EMImBF_4$ system and also showed low electrode/electrolyte interfacial resistance. Consequently, this novel CS-TFE is suitable for high-performance EDLCs and improves the safety of such devices.

In chapter 4, A novel nanofibrous gel electrolyte was prepared via gelatin electrospinning to be used as a nonaqueous electrolyte in EDLCs. An electrospinning technique with a 25 wt% gelatin solution was used to produce gelatin electrospun (GES) electrolytes. A structural analysis of the GES products showed a clearly nanofibrous structure having fiber diameters in the range of approximately 306.2–428.4 nm, high thermal stability, high tensile strength, and resistance to damage upon immersion in $EMImBF_4$. After testing a range of spinning times, GES electrolytes that were electrospun with 25 min of spinning time (GES-25) were used to fabricate EDLC test cells with $EMImBF_4$. These test cells were compared with test cells using gelatin films containing $EMImBF_4$ and with testing cells using pure $EMImBF_4$ with a separator as the electrolyte. The test cell with the GES-25/$EMImBF_4$ gel electrolyte showed a similar IR drop and discharge capacitance as the liquid-$EMImBF_4$ test cell. However, the electronic contact resistance in activated carbon electrode at the electrode/electrolyte interface was significantly better in the GES-25/$EMImBF_4$ test cell compared with the test cell with the gelatin film/$EMImBF_4$ electrolytes. The results demonstrate that this novel nonaqueous gel electrolyte can be used for solid-stage electrolyte in EDLCs to improve the safety of such devices.

List of Publication

List of Publication

1. Preparation and characterization of gel electrolyte with bacterial cellulose coated with alternating layers of chitosan and alginate for electric double-layer capacitors, D. Kotatha, K. Morishima, S. Uchida, M. Ogino, M. Ishikawa, T. Furuike and H. Tamura, *Research on Chemical Intermediate*, 44, 4971–4987 (2018).

2. Preparation and characterizations of thin-film electrolyte from chitosan containing ionic liquid for application to electric double-layer capacitors, D. Kotatha, K. Shinomiya, Y. Torii, M. Ogino, S. Uchida, M. Ishikawa, T. Furuike and H. Tamura, *International Journal of Biological Macromolecules*, accepted

3. Preparation and characterization of electrospun gelatin nanofibers for used as nonaqueous electrolyte in electric double-layer capacitor, D. Kotatha, M. Hirata, M. Ogino, S. Uchida, M. Ishikawa, T. Furuike and H. Tamura, Submitted to *Journal of Nanotechnology* (2018.08.31)

Acknowledgments

Acknowledgements

This thesis would have been impossible without the help form my advisor, Professor Dr. Hiroshi Tamura of Department of Chemistry and Materials Engineering, Faculty of Chemistry, Materials, Bioengineering, Kansai University. I would like to express sincere appreciation to Professor Dr. Hiroshi Tamura as he gave me a precious opportunity to be a PhD student under his supervision. And thank you for his continuous guidance, discussions and many encouragements throughout this study. Not only the academic part, he always gives me a lot of opportunities and many things to my life.

I would like to express my thanks to my co-advisor, Professor Dr. Tetsuya Furuike, Department of Chemistry and Materials Engineering, Faculty of Chemistry, Materials, Bioengineering, Kansai University, for his kindness and helpful, useful discussions, advice and encouragement. Through his much valuable advice, I learned a great deal of scientific thinking.

I would like to express my thanks to Professor Dr. Masashi Ishikawa Department of Chemistry and Materials Engineering, Faculty of Chemistry, Materials, Bioengineering, Kansai University. And my team member in Electrochemical laboratory for excellent co-working, good advice and always support in part of electrochemical proprieties in this thesis.

I would like to express deepest gratitude to Nishimura scholarship foundation and also other foundations to support me during the past three years for studying in Japan. They are parts of the successful for my PhD life.

I would also like to thank to all of laboratory member in Biofuntionalize Chemistry Laboratory for the kindness and helpful in any situation, for stimulating discussions, for working hard together, and for all the fun in the last three years. It will be in my heart forever. Special thanks to my team members; Mr. Keito Shinomiya, Mr. Masaharu Hirata and Mr. Yoshiki Torii for every support and give me more happiness in PhD life.

Last but not least, I am very thankful to my family especially Mrs. Payom Kotatha and Mr. Jaturapon Kotatha for support, understand and believe me in everything that I choose, encourage and always beside me.

DITPON KOTATHA